



MINISTRY OF AVIATION

AERONAUTICAL RESEARCH COUNCIL
REPORTS AND MEMORANDA

Some Early Experiments on Vortex Separation

Part I.—Some Low Speed Aerodynamic Properties of Cones

By P. T. FINK

Part II.—Some Low Speed Experiments with 20 deg. Delta Wings

By P. T. FINK and J. TAYLOR

Part III.—Further Experiments with 20 deg. Delta Wings

By P. T. FINK

LIBRARY
ROYAL AIRCRAFT ESTABLISHMENT
RAF FARNBOROUGH

LONDON: HER MAJESTY'S STATIONERY OFFICE

1967

PRICE 19s. 6d. NET

Some Early Experiments on Vortex Separation[#]

*Reports and Memoranda No. 3489**

September, 1966

Part I.—Some Low Speed Aerodynamic Properties of Cones

By P. T. FINK[§]

Summary.

The results are presented of some low-speed wind tunnel tests on a right circular cone with apex angle 20 deg. and on elliptic cones with apex angles 60 deg. and 20 deg. The experiments included balance tests, measurements of pressure distribution and a limited amount of flow visualisation with tufts. The emphasis of the work has been on the range of angles of incidence for which viscous effects were appreciable. Symmetric and asymmetric vortex arrangements were found over the suction side of the right circular cone.

LIST OF CONTENTS

Section

1. Introduction
2. The Models
3. Measurements
4. Discussion

[#]This is a summary report of work done some years ago in the Imperial College Aeronautical Laboratory under the general supervision of the late Prof. H. B. Squire, F.R.S. Certain phenomena, including that of vortex bursting, remained undiscovered in these experiments and the writer had some hesitation about proceeding with publication in the R. & M. Series. However, the several parts of the present paper have been continually referred to by other workers; in particular, J. H. B. Smith's very important theoretical paper 'Improved calculations of leading-edge separation from slender delta wings,' A.R.C. 27 897, March, 1966, makes repeated reference to the experiments reported in Part II. It was therefore felt useful to proceed to permanent publication.

*Part I replaces A.R.C. 17 632.

Part II replaces A.R.C. 17 854.

Part III replaces A.R.C. 19 526.

[§]Now at Department of Mechanical Engineering, The University of Sydney.

1. Introduction.

A programme of experimental work on a family of cones and delta wings was begun in the 5 ft. \times 4 ft. low speed wind tunnel at Imperial College early in 1953. It was hoped to learn something of the nature of the flow which produces non-linear lift curves. The first set of measurements was made on two conical bodies. Separation of the cross flow and vortex shedding were observed and the results are presented in this report. It was thought useful to fix the separation at a known position and it was decided to continue the programme with experiments on a delta wing with sharp leading edges. The corresponding measurements of surface pressure and extensive total head traverses in the vortex region are reported.

2. Models.

Cone A. This was a right circular cone with apex angle 20 deg. and axial length 24 inches. The model was made of laminated teak and French polished. The nose piece, $1\frac{1}{2}$ inches long, was made of Tufnol. The cone was sting mounted on a wire suspension as is shown in Fig. 1. The cone was fitted with 56 flush-surface pressure orifices formed of $\frac{1}{16}$ in. o.d. copper tubing; their disposition is shown in Fig. 1. The coverage of these holes was extended by turning the cone about its axis through angles up to $22\frac{1}{2}$ deg. The connections to a multi-tube manometer were taken out of the base of the cone.

Cone C. This was an elliptic cone. The elevation was identical with that of cone A; the apex angle in plan was 60 deg. The construction was similar to that of cone A. The model was fitted with 122 surface pressure orifices and was mounted on a horizontal steel tube as shown in Fig. 2.

3. Measurements.

3.1. Measurements on Cone A.

Force measurements were made on a three-component balance as a routine preliminary. They led to the replacement of the original spear mounting by a wire suspension. The forward spread of the effect of the base made it impossible to derive much information from the balance measurements; e.g. the centre of pressure was found at $x/L = 0.45$. The surface static pressure was measured as follows:

Distribution of pressure along certain generators. The static pressure was measured at six stations in the rear two thirds of each of four generators for windspeeds of 100 ft./sec. and 160 ft./sec. at angles of incidence up to 30 deg. The chosen generators were at the 'top', 'sides' and the 'bottom' of the cone; i.e. $\theta = 0^\circ, 90^\circ, 180^\circ$ and 270° (Fig. 1). The distributions are shown plotted in Figs. 3, 4, 5 and 6.

Distribution of pressure at two chordwise stations. An extensive set of measurements was made at the forward station 6 and a smaller survey was made at the Station 3 (Fig. 1). The angle of incidence was in the range $-12^\circ \leq \alpha \leq 50^\circ$. The wind tunnel was run at speeds between 75 and 160 ft./sec. Some of the distributions obtained at Station 6 are shown plotted in Figs. 7 and 8 the first of which also contains a comparison with Allen's theory¹. The local coefficient of normal force C_{Nl} was obtained from all the above distributions. The values at Station 6 are shown plotted in Fig. 9. The coefficient of local side force C_{Yl} and the inclination to the vertical Φ of the resultant force $\sqrt{(N^2 + Y^2)}$ are given in Fig. 10.

Visualisation of the flow. A universal traverse gear was not built when these experiments were made and the tuft studies were not precise. Two vortex regions in which a tuft spun rapidly were found above the suction side of the cone for angles of incidence greater than 15 deg. This vorticity appeared to start indefinitely close to the nose of the cone. At 30 deg. incidence, the regions were $\frac{1}{8}$ in. \times $\frac{1}{8}$ in., $\frac{1}{4}$ in. away from the surface at $\theta = 180^\circ \pm 13^\circ$ all at Station 6. At a station 2 inches ahead of the base, the cores were larger and were situated about 1 inch from the surface at $\theta = 180^\circ \pm 18^\circ$. This outward drift is an expected motion of vortices near a boundary.

3.2. Measurements on Cone C.

The static pressure was measured at six stations in the rear two thirds of each of four generators at a wind speed of 75 ft./sec. and at angles of incidence up to 30 deg. The generators were situated at $\theta = 0^\circ, 37\frac{1}{2}^\circ, 142\frac{1}{2}^\circ$ and 180° (Fig. 2). The incremental pressure distributions are plotted in Figs. 12, 13. Detailed measurements of the distribution of pressure were also made at the (forward) station 6 for the range of angle of incidence $0^\circ \leq \alpha \leq 45^\circ$. The distribution at $\alpha = 5^\circ$ is plotted in Fig. 13 together with an

estimate from slender body theory. The distribution at higher incidence is shown in Figs. 14 and 15. The corresponding normal force curve is given in Fig. 17.

Vortex regions were found with tufts for angles of incidence $\alpha \geq 10^\circ$. The results of an attempt to map one of the regions is shown in Fig. 17. The experimental points noted were obtained by moving a tuft probe until the tuft just failed to spin. The tunnel had then to be shut down in order to mark the position of the probe on a template. Surface flow patterns were obtained with the paraffin-chalk technique and a typical picture is shown in Fig. 18a.

4. Discussion.

4.1. Cone A.

The distribution of pressure along certain generators. (Figs. 3, 4, 5 and 6). At zero incidence the pressure at the foremost Station 6 was found to be greater than free stream static ($c_p = 0.13$) as was consistent with the deflection of the stream. The pressure fell increasingly rapidly to its value $c_p = -0.27$ at the base. No Reynolds number effect was noticeable in the range tested.

The distributions at angles of incidence up to 30° change similarly along the generators. The incremental pressures $c_p - (c_p)_{\alpha=0}$ are nearly constant over the middle third of the cone. This result encourages one to have some confidence in the validity of cross-flow theories for this body so long as they are not applied too close to the base.

The distribution of pressure at two chordwise stations. Only the results for the forward Station 6 are produced here. At this station, the surface static is little subject to Reynolds number. In Fig. 7 a comparison with an estimate from inviscid slender body theory (Allen¹) is shown. An empirical $\Delta c_p = 0.128$ has been included to allow for the effect of thickness. Good agreement is found between this theory and experiment for $\alpha < 18^\circ$. At larger angles of incidence the effect of 'vortex separation' is marked and it is seen how the failure of the pressure to recover on the lifting side of the cone leads to enhancement of the lift. In Fig. 8 shows some distributions for $20^\circ \leq \alpha \leq 50^\circ$. Considerable asymmetry of the pressure distribution was found at angles of incidence in excess of 30° . This may not in fact involve more than a moderate change in the disposition of the vortices which form as a result of the separation of the cross flow. The precise position in which the vortices are stabilised at a given incidence and Reynolds number depends on the state of the boundary layers. It appears to change critically with small changes in the surface. It was found possible to *reverse* the asymmetry and also to abolish it by slight alterations of the orientation of a short piece of plastic tube which was held along the generator $\theta = 0$ near the apex of the cone.

The above distributions were integrated to evaluate the coefficients of local normal force C_{NI} and of local side force* C_{YI} as functions of incidence (Figs. 9 and 10). The scale effect is seen to be in the same sense that C_{NI} is reduced a little with increasing Reynolds number. The method of least squares was used to fit the following functions to the experimental points on Fig. 9.

(a) $C_{NI} = A \sin 2\alpha + B \sin^2 \alpha$, ($\alpha \geq 0$). This yielded $A = 0.62$, $B = 2.61$ and this is clearly a useless result.

(b) $C_{NI} = A \sin 2\alpha + B |\sin \alpha| \sin \alpha$ for $-6^\circ \leq \alpha \leq 9^\circ$. This yielded $A = 0.933$ and we deduce that the slope of the normal force curve attains 93 per cent of the Munk-Allen value in the above range of angles of incidence.

(c) $C_{NI} = 0.933 \sin 2\alpha + B \sin^2 \alpha$. This yielded $B = 1.68$ but the function does not fit the data and it may be concluded that the use of a constant cross flow drag coefficient B does not lead to useful results. Inviscid slender body theory predicts the movement of the suction peaks at the sides of the cone towards the pressure side with increasing incidence. One would therefore expect the cross flow drag coefficient to rise with increasing incidence at a station far downstream from the apex. At forward stations it is likely that the flow at a given angle of incidence is more like that past an expanding circular cylinder moving with constant velocity from an impulsive start.

*The side forces were worked out by Mr. D. A. Treadgold of the R.A.E.

(d) Kelly² quotes the results of Schwabe's indirect determination of the drag of a circular cylinder (of fixed diameter) which moves with constant velocity from an impulsive start. Kelly uses this to deduce cross flow drag coefficients for cone-cylinder and ogive-cylinder combinations and obtains good agreement with experiment. Kelly does not state that the analogy is incomplete for the non-cylindrical portions of his bodies but he attempts to allow for this by interpreting Schwabe's time parameter (velocity \times time/radius) as $[(U \sin \alpha)/r] [x/(U \cos \alpha)] = (x \tan \alpha)/r$ and inserting the correct ratio x/r everywhere along the body. That this procedure cannot replace the use of the correct analogy becomes plain by considering that a body of revolution with straight generators has constant $(x \tan \alpha)/r$ at any incidence and this leads to the use of only one point of Schwabe's time history of the drag regardless of the length of the cone. It is seen in Fig. 9 that the agreement of the present experiments with a Kelly-Schwabe theory is indifferent. The tests reported in Ref. 2 were on bodies whose cylindrical portions were much longer than their nose portions; i.e. the correct analogy was used for the major part of the bodies. Kelly's good agreement of theory and experiment probably derives from this cause.

It is seen in Fig. 10 that the side force which arises from the asymmetric disposition of the shed vorticity (Fig. 8) is an appreciable fraction of the normal force. At $\alpha = 50$ deg. the resultant force $\sqrt{(N^2 + Y^2)}$ is inclined 36 deg. away from the vertical.

4.2. Cone C.

The incremental pressure $c_p - (c_p)_{\alpha=0}$ varies appreciably along four generators (Figs. 11 and 12) at all but the smallest angle of incidence and it may be said that the flow over this body is not conical. However, the spanwise pressure distribution at 5 deg. incidence at Station 6 is in qualitative agreement with an estimate from inviscid slender body theory (Fig. 13). The distribution of pressure at this station for angles of incidence up to 45 deg. is shown in Figs. 14 and 15). The development of peaks of suction under the vortices is clearly seen for angles of incidence in excess of 10 deg. The peaks become smaller in magnitude at 40 deg. incidence when something like a conventional stall begins. This is also evident in the corresponding local normal force curve (Fig. 16). The slender wing estimate $C_{NI} = \alpha \frac{\pi}{2}$ (Aspect Ratio) is marked. This coefficient is based on plan area.

The map of the vortex region shown in Fig. 17 illustrates how boundary-layer fluid is washed into the stream ('separation of the cross-flow') to feed a vortex core. In later work tuft surveys have been compared with total head surveys. It appeared that the former gave a much less accurate impression of the phenomena than the latter. The boundary shown dotted in Fig. 17 should therefore be treated as being merely qualitatively correct.

The surface flow pattern at $\alpha = 30$ deg. (Fig. 18a) shows the large angles of yaw which obtain under the main vortex core. The 'primary' separation near the leading edge cannot easily be seen in the photograph but it was evident in side view. A 'secondary' separation is seen to take place outboard of the strongly yawed flow under the vortex. The chalk pattern discloses the presence of a limited extent of reversed yaw while further outboard the surface flow is again yawed towards the edge and it seems that a re-attachment has taken place. The air approaches the primary separation line turns and is entrained by air from the pressure side to 'feed' the main vortex further downstream. These directions of flow are sketched in Fig. 18b. They are not inconsistent with the pressure distribution shown in Figs. 14 and 15.

REFERENCES

- | <i>No.</i> | <i>Author(s)</i> | <i>Title, etc.</i> |
|------------|-------------------|---|
| 1 | H. J. Allen | Pressure distribution and some effects of viscosity on slender inclined bodies of revolution.
NACA Tech. Note 2044, March 1950. |
| 2 | H. R. Kelly | The estimation of normal-force, drag and pitching-moment coefficients for blunt-based bodies of revolution at large angles of attack.
<i>J. Aeronaut. Sci.</i> , Vol. 21, pp. 549-555 and 565. 1954. |

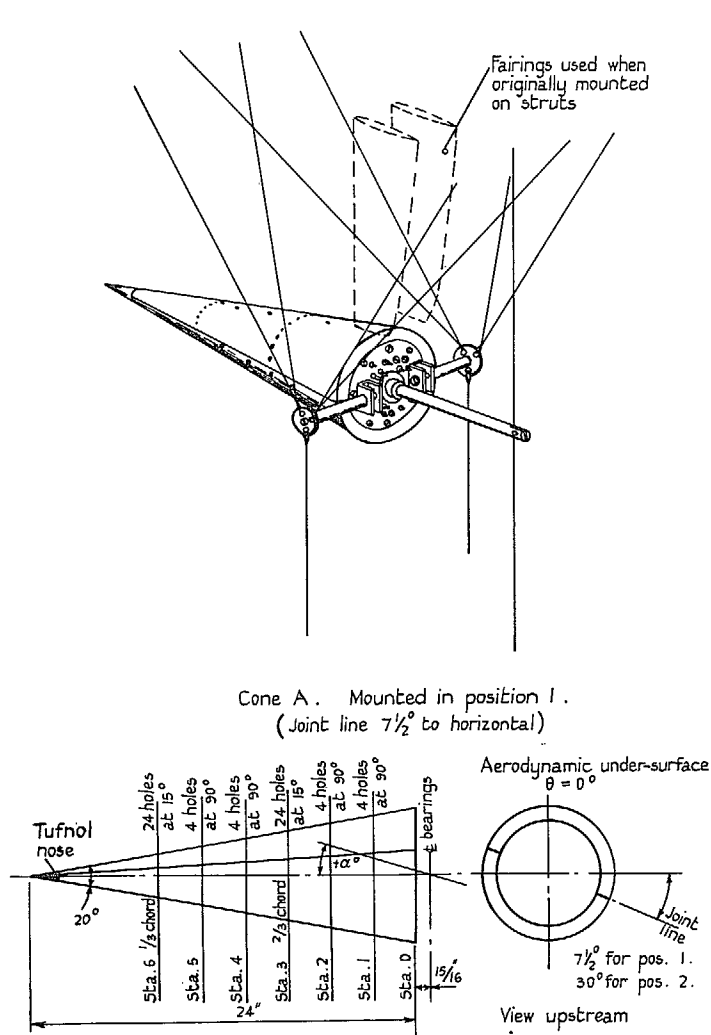


FIG. 1. Cone A. Mounted in position 1.
(Joint line $7\frac{1}{2}$ deg. to horizontal).

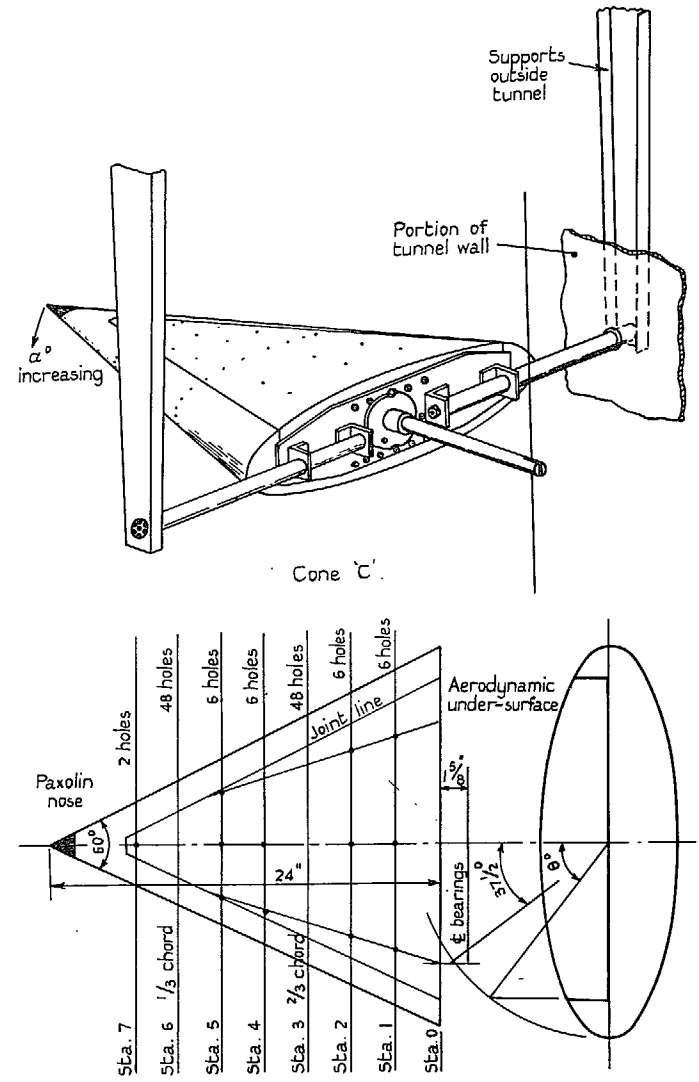


FIG. 2. Model supports and disposition of pressure holes.

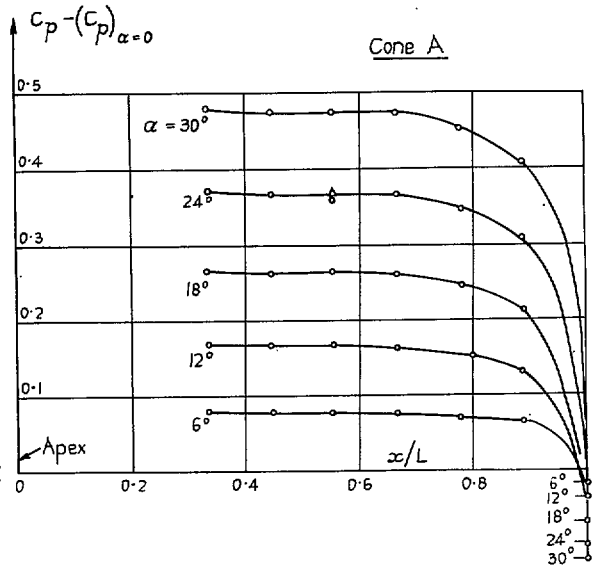
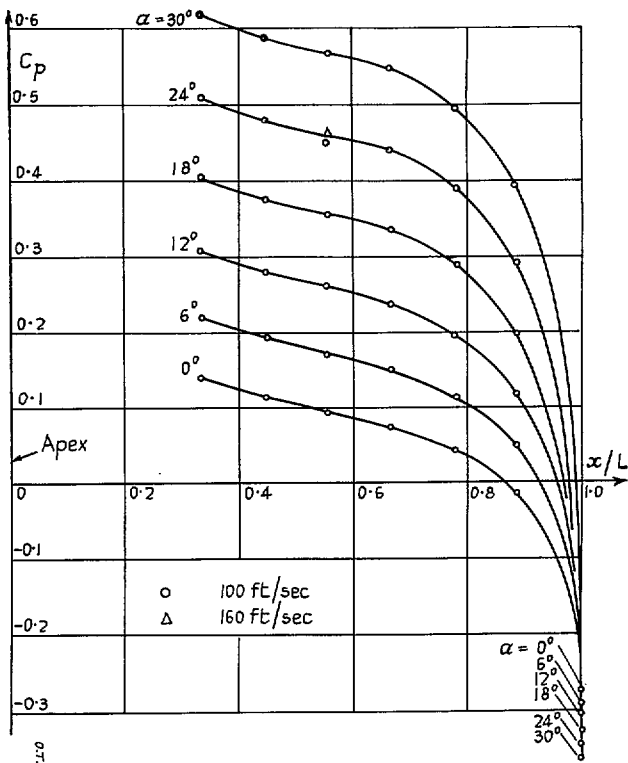


FIG. 3. Distribution of pressure for the generator $\theta = 0$ deg.

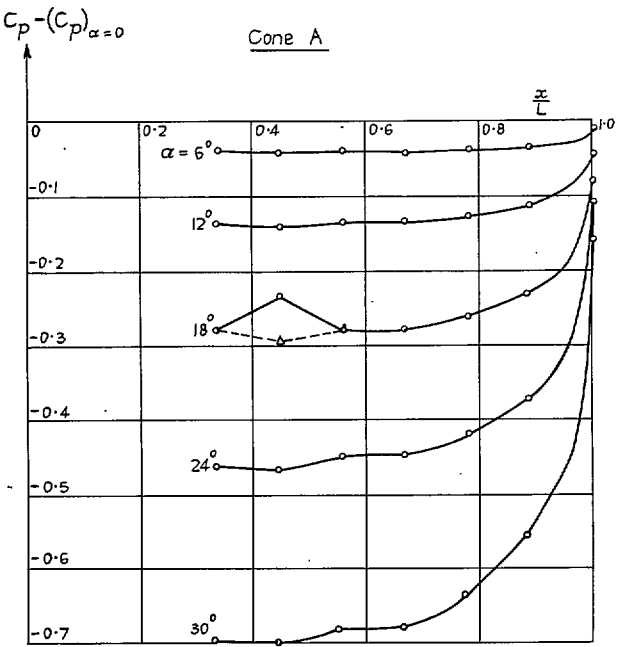
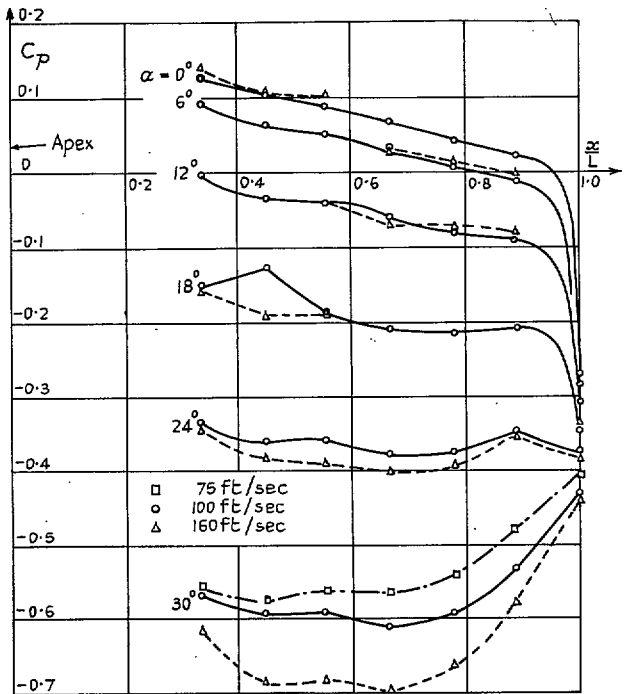


FIG. 4. Distribution of pressure for the generator $\theta = 90$ deg.

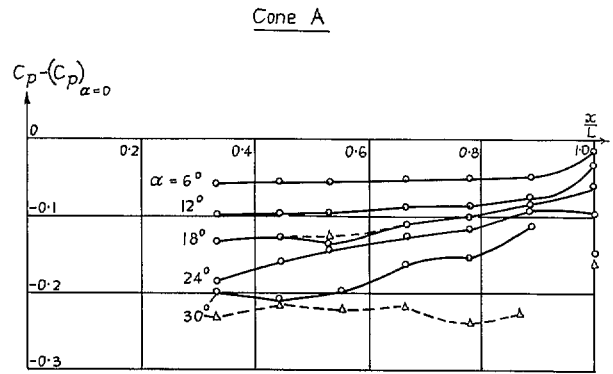
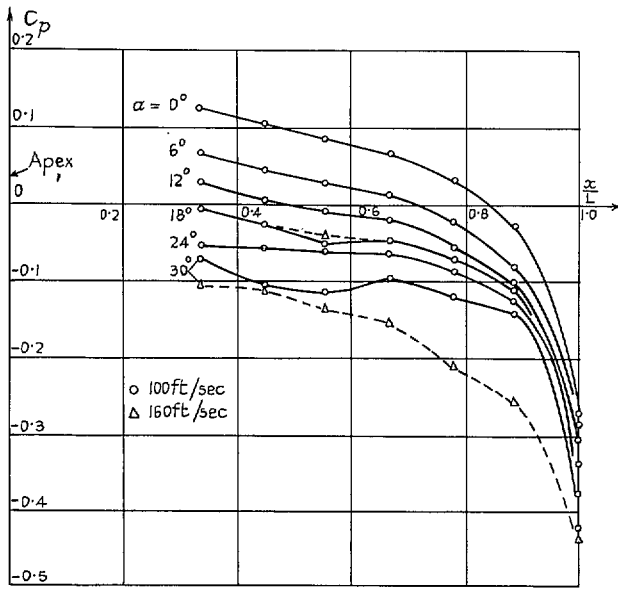


FIG. 5. Distribution of pressure for the generator $\theta = 180$ deg.

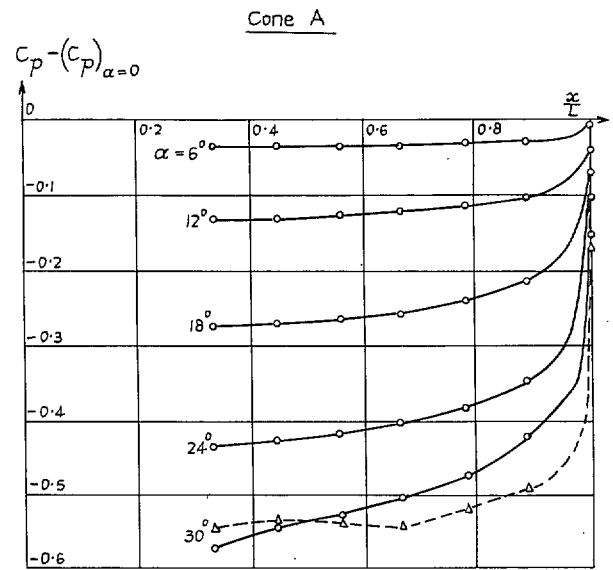
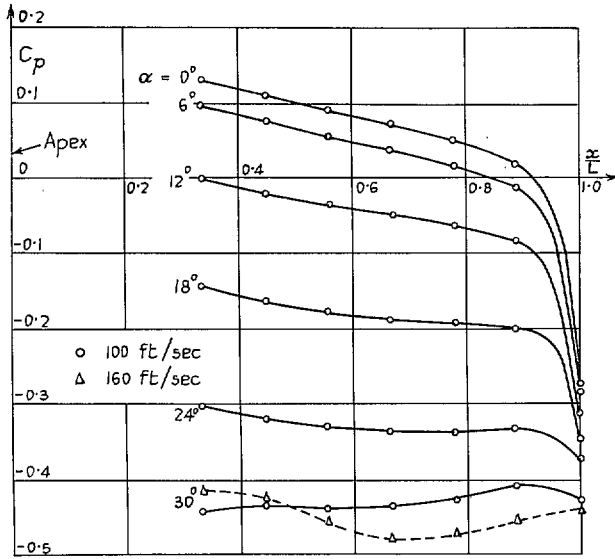


FIG. 6. Distribution of pressure for the generator $\theta = 270$ deg.

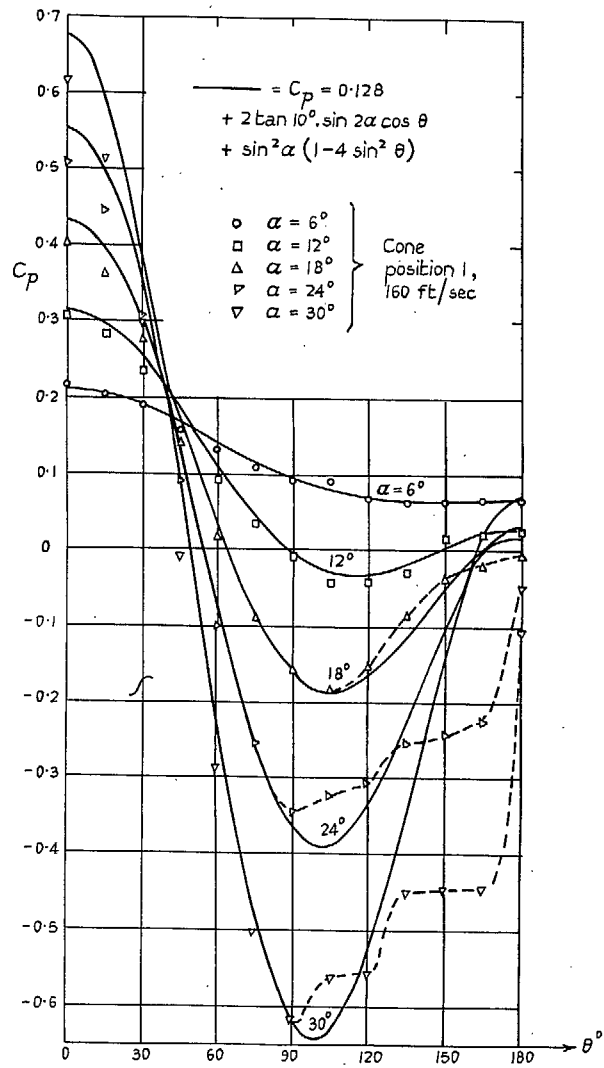


FIG. 7. Pressure distribution at Sta. 6: comparison with inviscid slender body theory. Cone A.

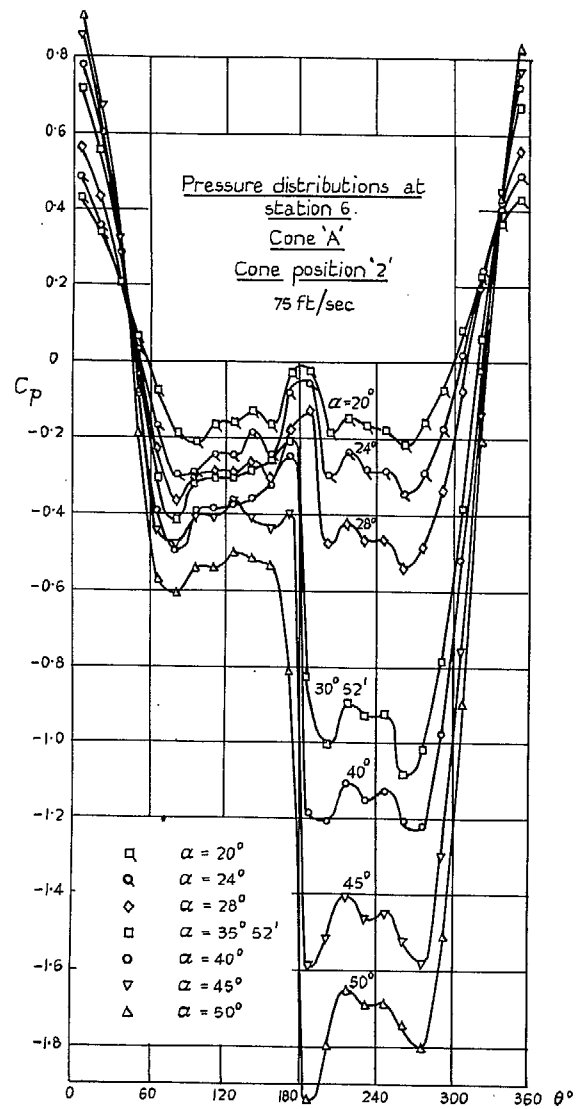


FIG. 8. Pressure distribution at Sta. 6: Cone A. Cone position '2'. 75 ft/sec.

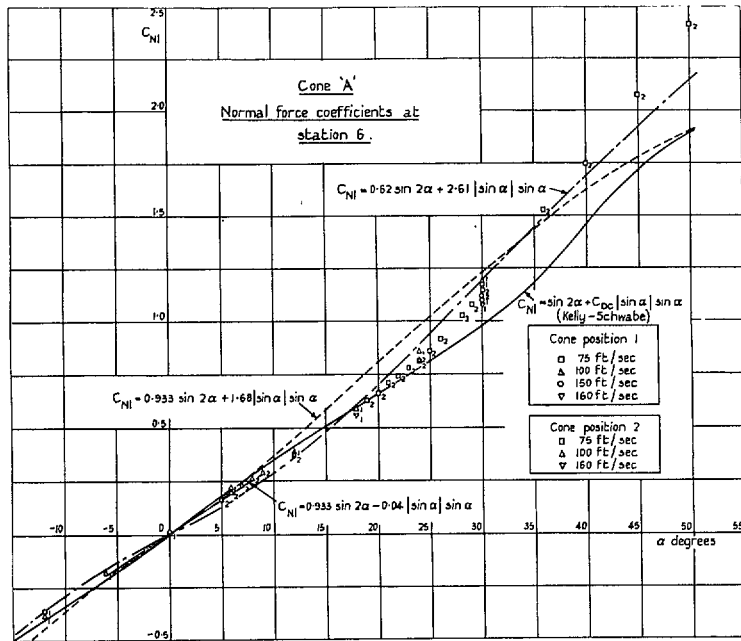


FIG. 9. Cone A. Normal force coefficients at Sta. 6.

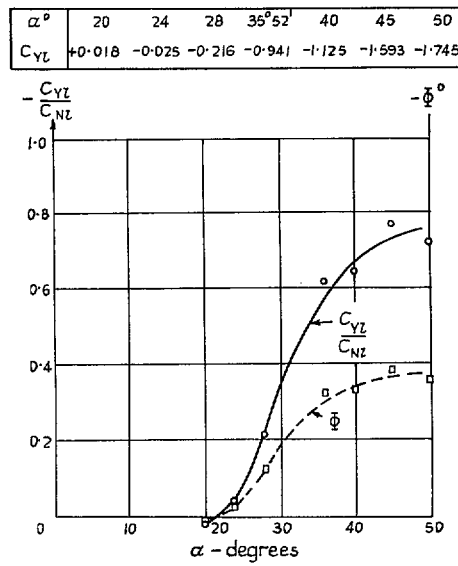


FIG. 10. Cone A. Side force at Sta. 6.

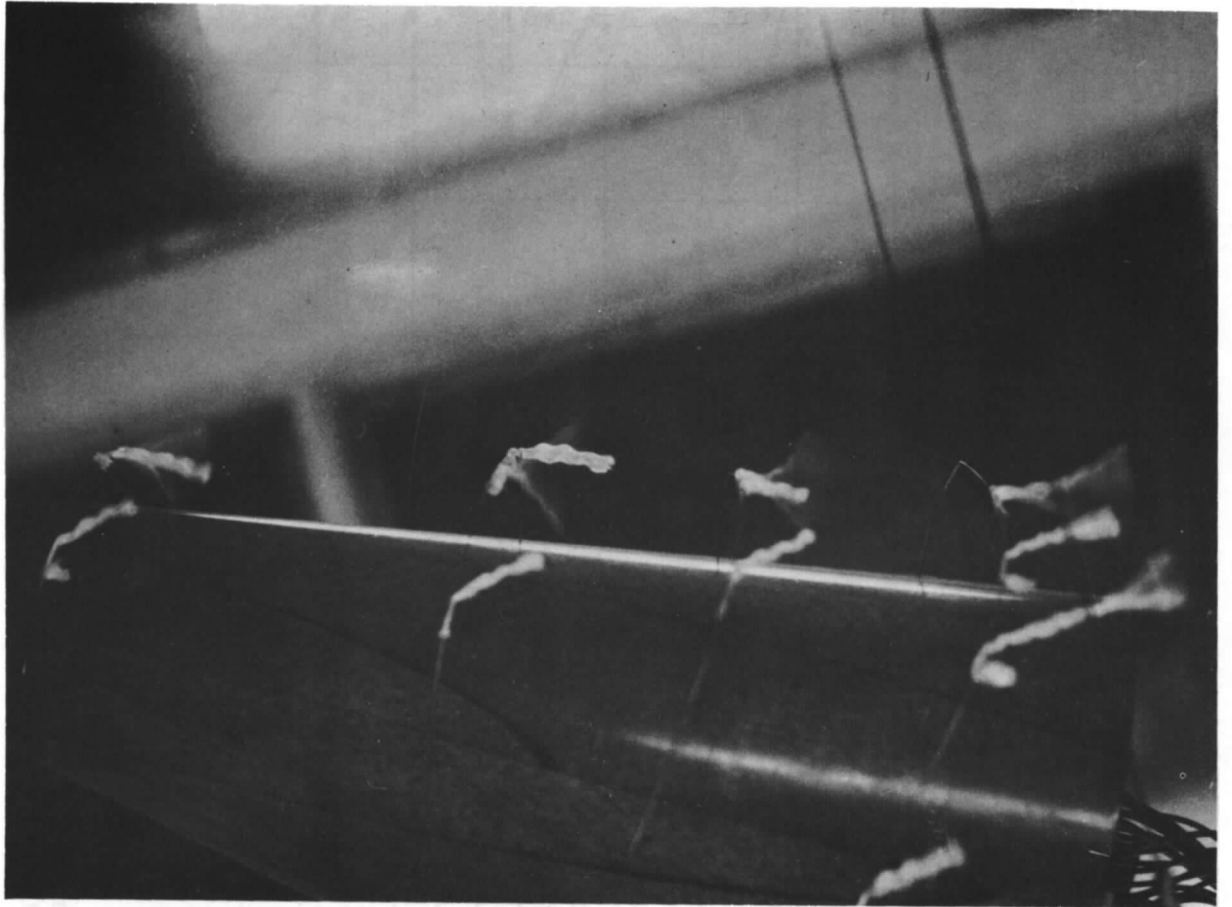


FIG. 11. Cone A: 30° incidence.

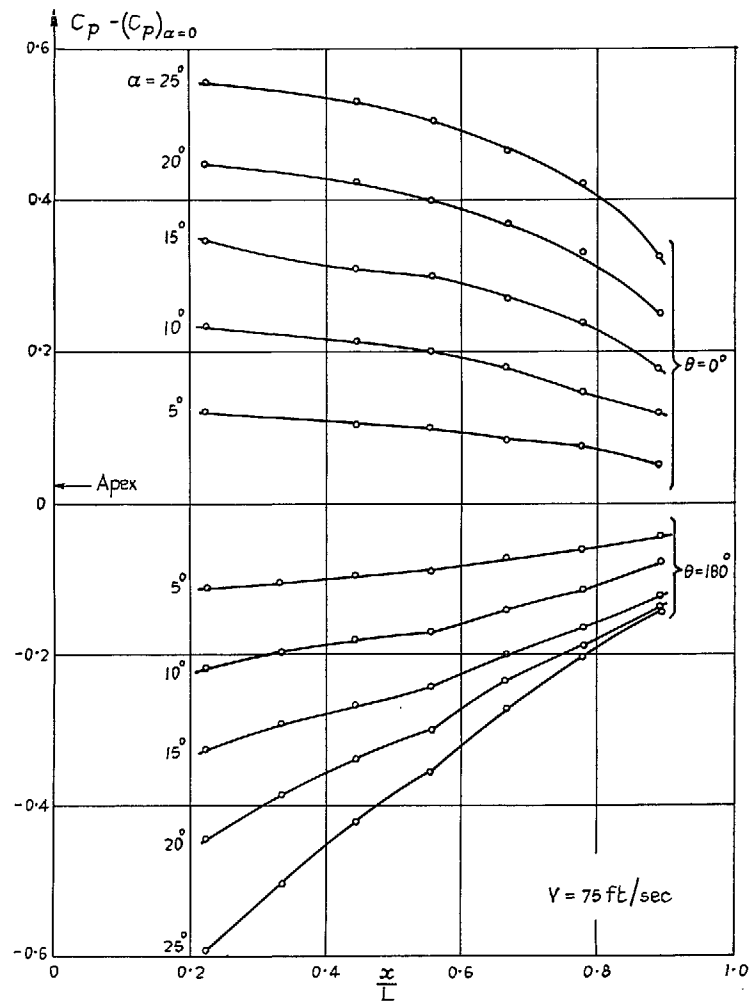


FIG. 12. Distribution of incremental pressure for the generators $\theta = 0^\circ, 180^\circ$.

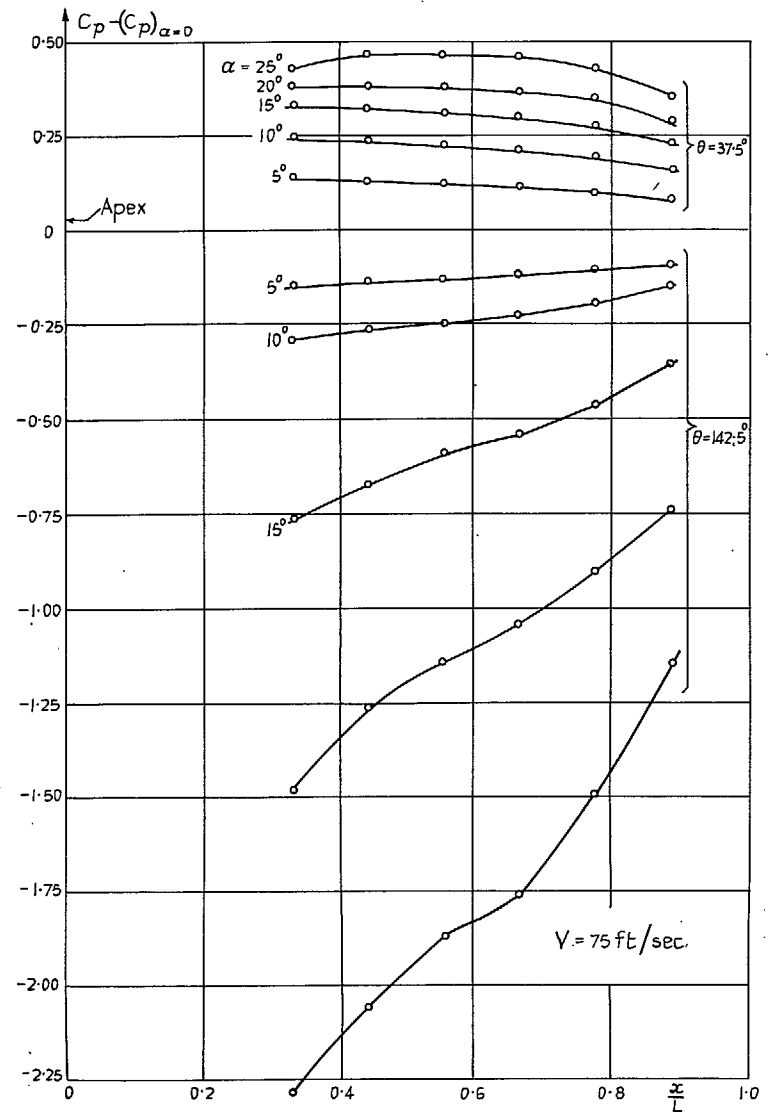


FIG. 13. Distribution of incremental pressure for the generators $\theta = 37.5^\circ, 142.5^\circ$.

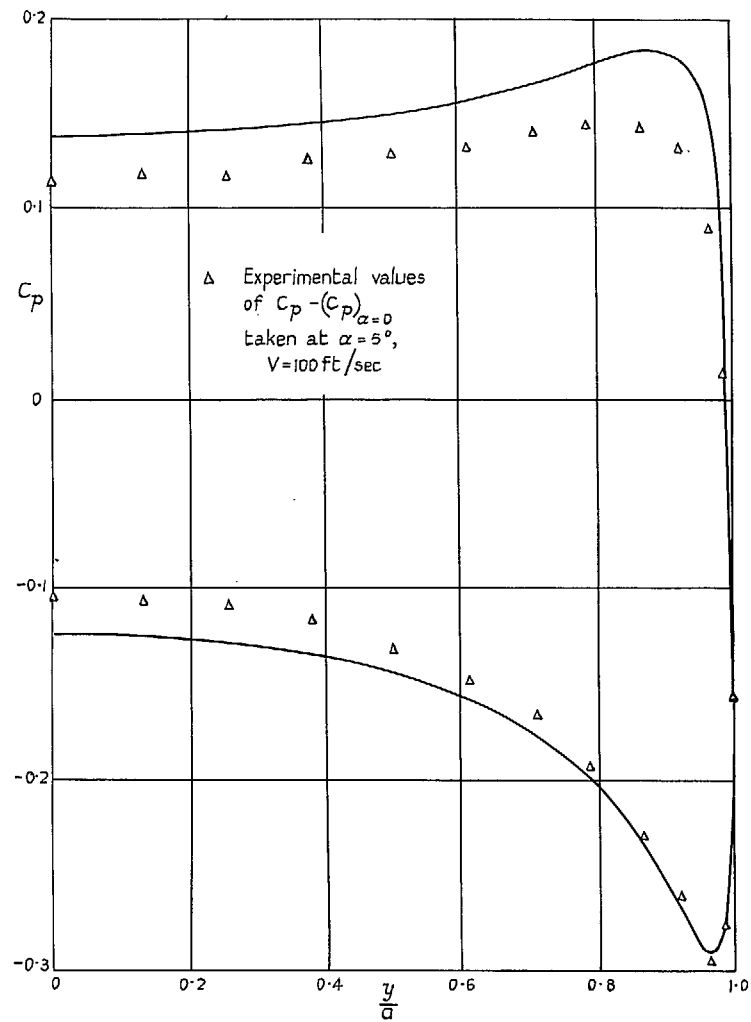


FIG. 14. Pressure distribution at Sta. 6: Comparison with inviscid slender body theory.

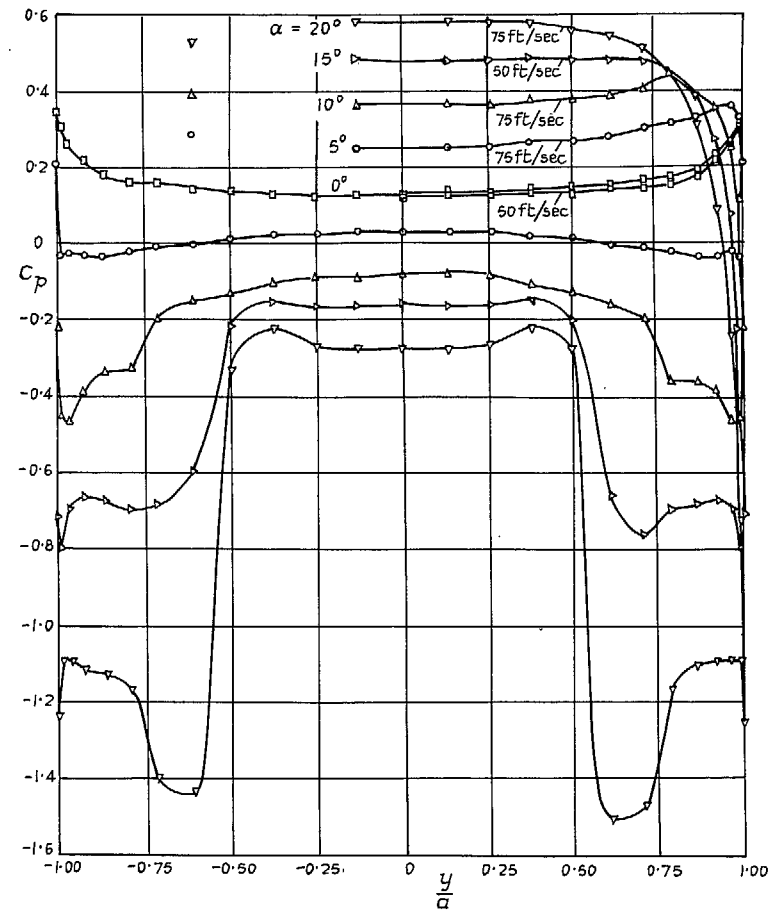


FIG. 15. Distribution of pressure at Sta. 6.

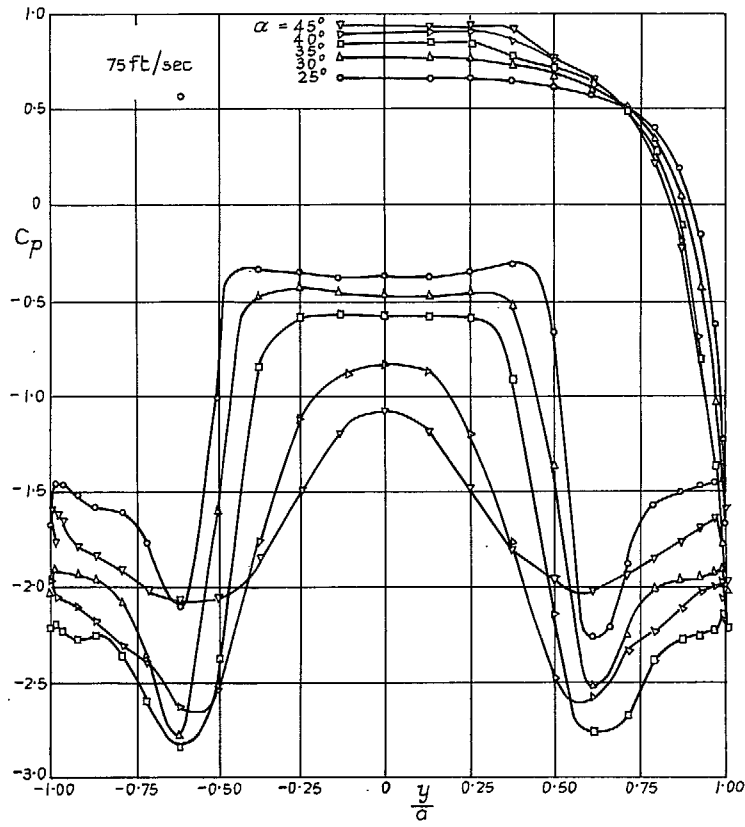


FIG. 16. Distribution of pressure at Sta. 6.

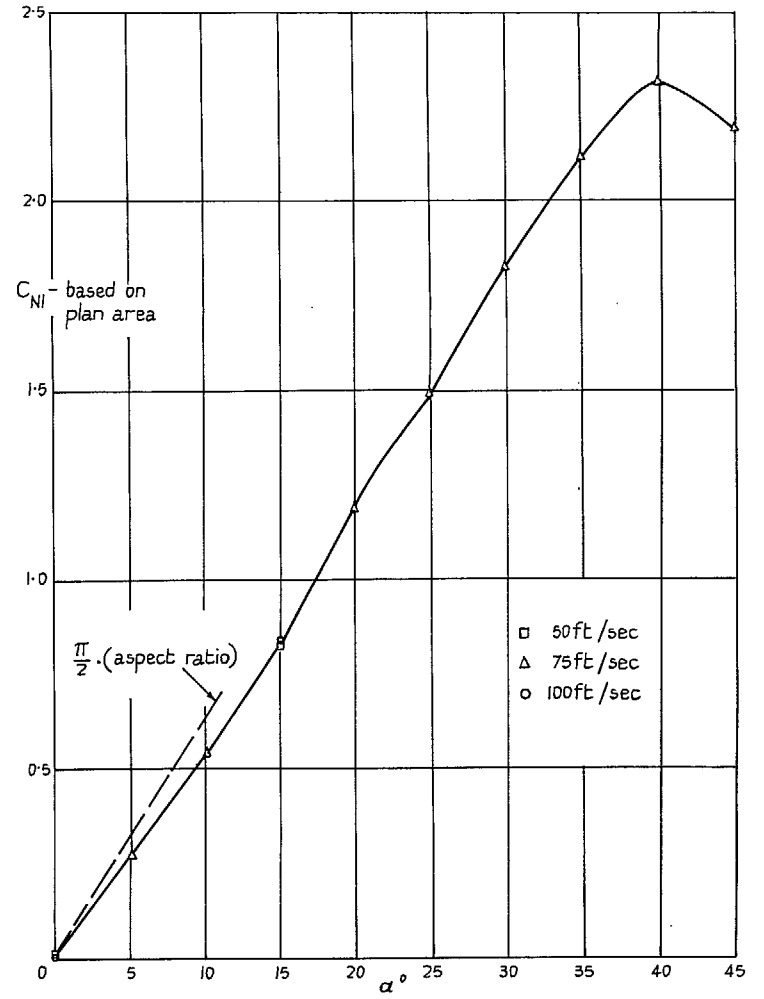


FIG. 17. Normal force at Sta. 6.

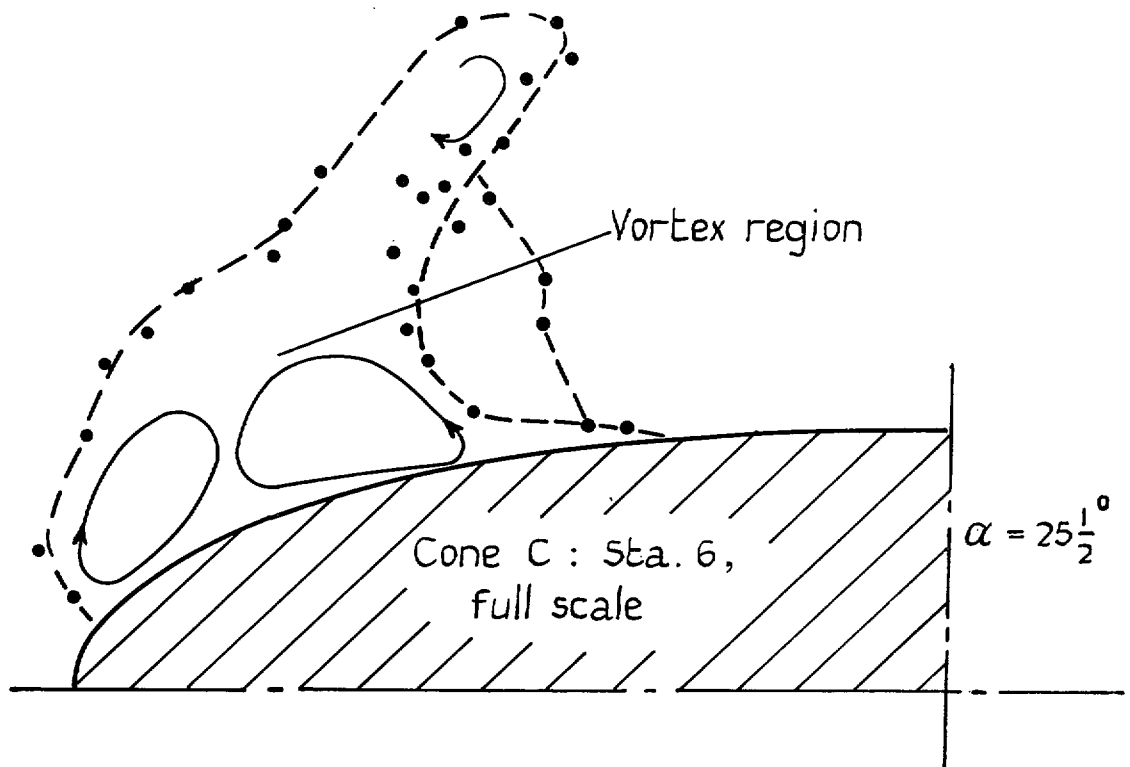
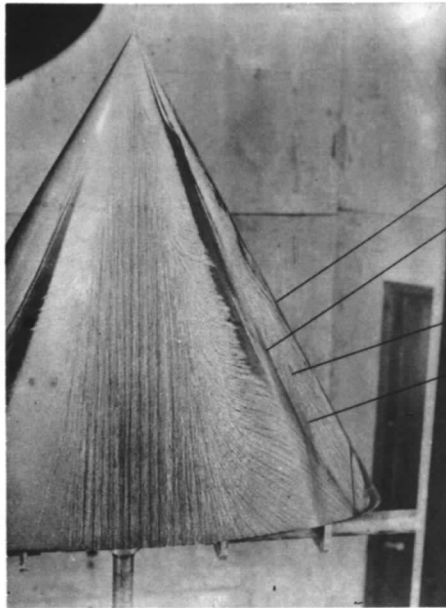
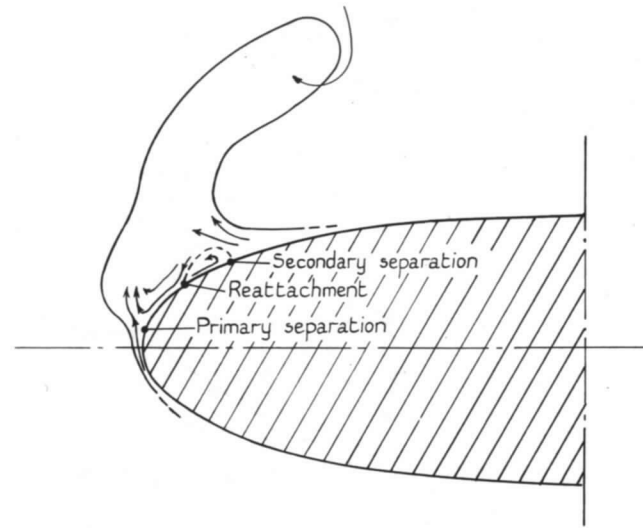


FIG. 18. Flow visualisation with tufts.



Primary separation
Secondary separation
Reversed yaw
Reattached flow

FIG. 19a.



Secondary separation
Reattachment
Primary separation

FIG. 19b.

Part II.—Some Low Speed Experiments with 20 deg. Delta

By P. T. FINK and J. TAYLOR

Summary.

The results are presented of some low speed wind tunnel tests on two delta wings with sharp leading edges which have 80 degrees sweepback. Leading edge separation and vortex formation on the suction sides of the wings were found at angles of incidence in excess of three degrees. The experiments included balance tests, measurements of surface static pressure along seven generators and at two chord stations, the determination of contours of constant total pressure in the vortex region and some flow visualisation with tufts, smoke, oil and a paraffin and chalk mixture.

LIST OF CONTENTS

Section

- 1 Introduction
- 2 Apparatus
 - 2.1 Models
 - 2.2 Traverse Gear
- 3 Balance Measurements on Model E1
- 4 Measurement of Pressure Distribution
- 5 Total Head Traverses
 - 5.1 Wing E1
 - 5.2 Wing E2
 - 5.3 Model D
- 6 Flow Visualisation
- 7 Concluding Remarks
- 8 Acknowledgments

1. Introduction.

At the conclusion of an experiment with a 20 deg. right circular cone which had been used to study vortex separation*, it was decided to construct a sharp edged delta wing. The cross-flow separation was to be fixed at the sharp edges, thus producing more instructive results than had been obtained from the cone. A large angle of leading edge sweep was chosen in the hope of obtaining a measure of approximately conical flow. The theory of R. Legendre¹ had appeared and improvements to it^{2, 3} were published as the work progressed. The wing was to be kept nearly flat in order to test this theory experimentally.

*See Part I.

After preliminary force measurements, the pressure was measured along some generators in order to determine the extent to which the flow was approximately conical. It was found that the influence of the trailing edge did not spread appreciably forward of the aft third of the wing in the range of incidence of the tests. The spanwise pressure distribution was then measured at two chord stations for several angles of incidence. Pressure minima were found on the suction side of the wing but the recovery of pressure outboard of the points of peak suction was always slow. Comparison with Legendre type theories showed that the local normal force agreed moderately well but that the details of the pressure distribution were incorrectly predicted.

Further facts about the flow were obtained in an extensive series of total pressure surveys over the suction side of the wing. It was found that the flow separated from the wing at the sharp leading edges for all but the smallest angles of incidence but it was more complicated than expected in that further separation of the cross flow took place on the suction side of the wing somewhat inboard of the leading edges. This 'secondary' separation was first reported by Ornberg⁴. Cross flow reattachment was noticed almost on the leading edges. Smoke and other methods of flow visualisation were then used in order to provide evidence for a consistent model of the flow.

These experiments were made in the 5 ft. × 4 ft. wind tunnel at Imperial College in 1954. The principal results of the measurements are outlined here.

2. Apparatus.

2.1. Models.

Model E1. This was a flat plate delta wing with apex angle 20 deg. and root chord 24 in. (Fig. 1). It was made of 10 S.W.G. (0.128 in.) duralumin. Both surfaces had a constant chamfer of $\frac{3}{4}$ in. parallel to the leading edges – i.e. not along generators – from a point 4.32 in. downstream of the apex. The included angle of the chamfer was 8.5 deg. The leading edge thickness was 0.013 in.

Tubes were laid along seven generators on one surface of the wing and 91 holes were drilled into them as static pressure orifices. Sellotape was used to seal the orifices which were not in use. Spanwise sawcuts were made from the leading edges to the outer tubes in order to measure pressure outboard of the latter tubes. The contour of the wing was preserved with Sellotape (0.002 in. thick) and holes were pierced through a jig at the points where the pressures were to be measured. The Sellotape was renewed between measurements. A sting was attached at the rear of the model and this was supported by a wire suspension from the three-component balance.

Model E2. This was a flat plate delta wing whose planform, thickness and material were identical with those of the model E1. It differed in that one surface had been kept flat. The other surface had a constant chamfer of 1.50 inches parallel to the leading edge from a point 8.65 inches aft of the apex. The angle of the chamfer was $4\frac{3}{4}$ degrees. The leading-edge thickness was 0.009 inches. The spanwise sections of the wing ahead of the join of the chamfers were isosceles triangles. This wing was supported by a faired strut as is shown in Fig. 2. After this photograph was taken a slot was milled in the flat side at Station 1 (Fig. 1). This was connected to a chordwise slot in the chamfered side by a drilled hole. Both slots were covered with Sellotape and the spanwise pressure distribution at station 1 was obtained by piercing the Sellotape as described previously.

Model D. This was a 60 deg. delta wing of R.A.E.102 aerofoil section. The root chord was 2 ft.

2.2. Traverse Gear.

A traverse gear was arranged to move probes in the working section of the tunnel as follows:

- (i) 24 in. horizontally in the direction of the stream,
- (ii) 24 in. horizontally in a direction perpendicular to the stream,
- (iii) $9\frac{1}{2}$ in. vertically.

The latter two movements were made by continuous remote operation and could be repeated to 0.005 in. and 0.0005 in. respectively. Springs were used in the mechanism in order to eliminate backlash.

The traverse gear was used to probe vortex regions with swan's down tufts whose state of rotation was observed from outside the tunnel with a telescope. A Kiel probe was mounted on the traverse gear in order to make total head surveys of the vortex regions. The details and the calibration of the Kiel tube are shown in Fig. 3. It is seen that the tube was insensitive to yaw angles of less than 35 deg.

3. Balance Measurements on Model E1.

Preliminary force measurements were made on model E1 at a Reynolds number of 1.0×10^6 (based on the root chord). The results are given in Fig. 4, where the angle of incidence is used as independent variable for plots of the normal force coefficient C_N , chordwise force coefficient C_c and centre of pressure position C_p downstream of the apex expressed as a fraction of the root chord. The R. T. Jones values of C_N are given for reference. The variation of the lift/drag ratio with incidence is also shown.

The C_N curve has the characteristic departure from the simple slender wing theory of R. T. Jones and the measured value of C_N exceeds that of this theory by 50 per cent at an angle of incidence $\alpha = 10$ deg. The chordwise force is relatively small*, $0.018 \leq C_c \leq 0.039$ for $0^\circ \leq \alpha \leq 20^\circ$, and it is always directed away from the apex. This is an indication that the leading-edge suction is weak or absent and that the drag of the wing is high. The maximum $L/D = 3.68$ and occurs at an angle of incidence of 9 deg. Beyond that incidence the function tends asymptotically to $\cot \alpha$ as expected.

If one attempts to fit the conventional performance equation

$$C_D = C_{D_0} + \frac{C_L^2}{\pi A e} \text{ for } \alpha \leq 30^\circ$$

one finds that the factor e changes considerably with incidence, viz.,

α°	5	10	15	20	25
e	0.38	0.61	0.72	0.81	0.75

The centre of pressure is 0.61 of the root chord downstream of the apex for the range of angles of incidence considered. This is about 6 per cent of root chord ahead of the slender wing estimate. The effect is due to the loss of lift near the trailing edge which is described in the next section. The apparent forward shift of the centre of pressure at very low incidence is thought to be due to a slight irregularity in the model.

4. Measurement of Pressure Distribution.

In the first place the surface static pressure was found along seven rays passing through the apex of the wing E1 in order to determine whether there were stations at which the pressure distribution might be taken to be approximately two-dimensional. It was immediately found that the upstream effect of the trailing edge was considerable. The flow cannot truthfully be described as a conical one even though the wing was quite slender but it may be seen from Figs. 5, 6, 7 and 8 that for angles of incidence not in excess of 15 deg. the pressure changes slowly along the rays over the middle third of the wing**. The Figures show the incremental pressure distribution $c_p - (c_p)_{\alpha=0}$. The pressure coefficient at zero incidence is in the range $0.04 \leq (c_p)_{\alpha=0} \leq 0.06$ at all test points. The 'base' pressure was not measured on wing E1 but the Figures give an indication of the manner in which the loading falls towards zero at the trailing edge.

*It was found that less than 1 per cent of C_c was attributable to the force on the 'base' of the wing.

**After this section had been written, Mr. G. H. Lee reminded the writer of the usefulness of the isobar presentation of pressure over a wing surface. The Fig. 8a was then prepared, showing isobars on the suction side of the wing E1 at $\alpha = 10$ deg. These support the conclusions drawn above.

The spanwise pressure distribution was then measured for the angles of incidence $\alpha = 5^\circ, 10^\circ, 15^\circ, 20^\circ, 25^\circ$ and 30° at the forward Station 1 and at Station 12, i.e. at $x/L = 0.292$ and 0.833 respectively (Figs. 9 and 10). It had been shown by other methods that vortex separation of the flow from the leading edges was present for this range of incidence. The minima of pressure shown correspond with the position of the vortex cores, being a little inboard of the latter. The flow has a component of velocity towards the leading edge here (Fig. 25). This disappears further outboard, the boundary layer thickens rapidly and we may think of the cross flow suffering a separation. The pressure rises slowly in this region. These features were found at both stations, the suction and the pressure being rather less near the trailing edge than further forward. The slight spanwise asymmetry of the pressure is thought to be due to misalignment of the model in yaw: the corresponding rolling moment at $\alpha = 10$ deg. was found to be one twentieth of that due to 10 deg. of yaw at 10 deg. incidence.

Most of the traversing over the suction side of the wing was done with model E2 and it was decided to check the effect of removing the chamfer from one surface by making a few surface static pressure measurements on E2. Distributions at $\alpha = 15^\circ$ and 30° for Station 1 on this model are shown in Fig. 12. The technique had been improved somewhat at this stage of the work and the results shown in Fig. 12 are considered to be more reliable than previous pressure measurements. The absence of chamfer on the suction side of the wing appears to increase the extent of the constant pressure region outboard of the suction peaks. In other respects the results are quite comparable with those on wing E1.

The coefficients of local normal force C_{NI} were found by integration of the surface pressure and values for Stations 1 and 12 are shown in Fig. 11. The balance measurements of normal force coefficient are given for reference. Possibly this may serve as an empirical guide to the relationship between local section properties at chordwise stations and overall (low speed) measurements. The following table of values also serves to give a comparison with some of the available theories.

Incidence (degrees)	5	10	15	20	25	30	
Wing E1 {	Sta. 12, C_{NI}	0.11	0.24	0.41	0.59	0.79	0.99
	Balance C_N	0.12	0.30	0.51	0.75	0.97	1.23
	Sta. 1, C_{NI}	0.14	0.34	0.61	0.93	1.28	1.66
Wing E2	Sta. 1, C_{NI}			0.63			1.55
R. T. Jones	0.10	0.19	0.29				
Legendre ¹ -Adams	0.21	0.56	0.91				
Edwards ²	0.15	0.35	0.59				
Brown-Michael ³	0.16	0.39					

It is thought that the values of C_{NI} obtained at Station 1 on wing E1 are the least unsuitable for comparison with (conical flow) theory. The R. T. Jones values are merely included for reference. The Legendre theory—including a correction due to Mac C. Adams—is seen to give values considerably in excess of measured values of C_{NI} . In the theories of Edwards² and Brown and Michael³ an attempt is made to take some account of the edge vortex sheets which connect the leading edges and the shed vortices. This produced quite good agreement with the experimental values of C_{NI} although the details of the spanwise pressure distribution were not reproduced. We may note the worst discrepancy: the Brown

Michael theory predicts a surface peak pressure coefficient $c_p = -1.56$ at 15 deg. incidence whereas the observed value was $c_p = -0.69$.

5. Total Head Traverses.

The traverse gear described in Section 2.2 was used to obtain contours of constant total head in regions of interest near the wings E1, E2 and the 60 degree delta model D. The quantity plotted in Figs. 13 to 20 and 21b is $(H - A)/(H_0 - A)$, H and H_0 are the measured values of total pressure at a point and in the free stream respectively. The atmospheric pressure A has been taken as a convenient reference pressure. The free-stream static pressure is in fact close to A so that the contours may be interpreted as lines of constant $(H - p_0)/\frac{1}{2}\rho V_0^2$ in the usual notation. All the traverses were made at a wind speed of 80 ft./sec.

5.1. Wing E1.

A limited amount of traversing was done in a vertical plane at a chord station 10 in. aft of the apex of E1, the model which had been used for most of the measurements of pressure distribution. The results for 5 deg. and 15 deg. incidence respectively are shown in Figs. 13 and 14. It is seen that the low incidence was barely sufficient to lead to vortex formation. The contours taken at the larger angle of incidence show the effects of leading edge separation in some detail. These features will be considered in the next Section. When it became apparent that a secondary separation took place on the suction side near $y/a = 10.7$ it was decided to build the wing E2 with one completely flat surface. This was meant to eliminate the possibility that the secondary separation was triggered off by the chamfer.

5.2. Wing E2.

Total head surveys in a vertical plane at a station 41.7 per cent of root chord are given in Figs. 15 to 18 for the range of angles of incidence $3^\circ \leq \alpha \leq 15^\circ$. For $\alpha = 3$ deg., the flow is unseparated (Fig. 15) and is in fact akin to that specified in the theoretical model of R. T. Jones. For $\alpha \geq 5$ deg. the free stream total head contour $(H - A)/(H_0 - A) = 1.0$ is seen to be considerably removed from the surface of the wing.

The principal features of the *cross flow* are:

- (i) separation of the boundary-layer flow from the pressure side at the leading edges,
- (ii) formation of vortex cores in the stream from boundary-layer fluid which has left *both* surfaces of the wing upstream of the traversed station,
- (iii) 'secondary' separation of the suction side boundary-layer a little outboard of the main vortex core position,
- (iv) re-attachment of the cross-flow outboard of the secondary separation points.

It was found that increasing incidence leads to:

- (a) a movement of the main vortex cores away from the leading edges,
- (b) a progressive reduction of the total pressure in the vortex cores,
- (c) increased intensity of the vortex sheets which spring from the primary separation points,
- (d) progressive reduction of the boundary-layer thickness on the central portion of the suction side of the wing. It is thought that this is associated with the increasing acceleration of the fluid as the strength of the vortices rises.

Total head surveys were also made at stations 0.38 per cent and 24 per cent of root chord downstream of the trailing edge (Figs. 19 and 20) for $\alpha = 10$ deg. The former is seen to be similar to the survey taken further forward at the same incidence. The apparent thickening of the pressure side boundary layer at

the centre of the wing was due to the wake of the supporting strut (Fig. 2). The latter shows the interaction of the main vortices with the 'edge' vortex sheets and the wake from the base of the wing. In the absence of further feeding the edge vortex sheets roll up to form a second pair of vortices which lies outboard of the main cores at the station shown. Since the sense of the rotation of the vortices on each side of the wing is the same,* we may expect them to twist like the strands of two ropes trailing from the wing. There is some evidence for this in a smoke photograph which shows the sinuous form of the main cores in plan view (Fig. 23).

Measurements were made at one chord station ($x/L = 0.417$) to determine the movement of the vortex cores with changing incidence. The co-ordinates of the points of minimum total head at $\alpha = 5^\circ$, 7° , 10° and 15° are shown in Fig. 21. Theoretical estimates due to Legendre² and Brown and Michael³ are also shown. It is seen that the vortices appear well inboard of the calculated position. The corresponding surface suction peaks are further inboard still. In both theories the vorticity distribution on the suction side of the wing is represented in very approximate form and the secondary separation is ignored. It is possible that the inclusion of an approximate representation of the secondary separation in the Brown and Michael model will give better agreement with experiment.

The results shown in Fig. 21 were taken at only one chord station but they appear to be representative. The deviation of the dimensionless co-ordinates of the vortex core at x/L from their values at $x/L = 0.417$ is shown in Fig. 21a for $\alpha = 10$ deg. and it is not large. The accuracy of the points falls off towards the apex since the wing span becomes smaller while the diameter of the Kiel tube is fixed. Vertical strokes are used to indicate the ratio of the diameter of the inner tube of the Kiel probe as a percentage of the diameter of the inner tube of the Kiel probe as a percentage of the local semispan a .

Comparison of the total head surveys for the wings E1, E2 shows that the vortex regime was complete at a smaller incidence for E2 than for E1. This is probably due less to the flat side of E2 than to its smaller chamfer. At high incidence there is little difference. The main cores are similarly situated and the minimum total pressure is the same for both wings at $\alpha = 15$ deg. However, the secondary separation appears to be 'stronger' for the wing E1 and a reverse flow vortex core is discernible here (Fig. 14)—if not for the wing E2. This vortex was first described by Ornberg⁴. We may recall work on two-dimensional bubble separation which shows that the presence of a vortex in the bubble is associated with rising pressure towards the tail of the bubble and that the pressure remains nearly constant when no distinct vortex is formed. It is thought that this may apply here also since the 'reattachment' of the cross flow is presumably associated with strong mixing near the edge of the bubble here as in the two-dimensional case. The spanwise pressure distributions for the two wings conform with this argument as may be seen by examining the Figs. 9 and 12.

The total head survey on wing E1 at 15 deg. incidence also exhibited some irregularities in shape of the contours $(H - A)/H_0 - A = 0.85, 0.90, 0.95$ and 1.00 . These have not been satisfactorily explained but it may be noted that though they alter the appearance of part of the survey, the regions of appreciable total head gradient are the same for both wings.

5.3. Model D.

The 'conventional' 60 deg. delta wing model D was available and a single total head traverse was made in a vertical plane immediately downstream of the trailing edge with the model set at 15° incidence. A vortex was seen to spring from each leading edge at 60 per cent chord aft of the apex and the traverse (Fig. 21b) has some features in common with the traverses discussed in Section 5.2.

Professor Lighthill has suggested that slender delta wings with similar sections would be expected to show similar vortex patterns at angles of incidence which are a fixed proportion of the apex angles of the deltas. This condition ensures a constant relation between the rates of expansion and normal motion of the traces of the wings in fixed cross-flow planes.

The wing D was set at an angle of incidence which was one quarter of the apex angle. This delta was

*See Section 4 of Part III.

neither slender nor of the same section as wing E2 but the reader is referred to Fig. 16 where a total head traverse is shown for the wing E2 at an angle of incidence which was also one quarter of the apex angle. It is seen that the minimum of total pressure is similarly situated for both wings and that there are strong edge vortex sheets in each case.

6. Flow Visualisation.

(i) Tufts.

Some preliminary tuft studies were made with the wing E1. A short swan's-down tuft was attached to the traverse gear (Section 2.2) and regions of strong and weak rotation of the tuft were mapped. An example is shown in Fig. 22. Superimposed on this are some of the total head contours from Fig. 14. The main vortex core was found to be in nearly the same position by both techniques but the interpretation of the regions of weak rotation of a tuft remains imprecise.

(ii) Smoke.

Smoke was introduced in a crude manner at a forward position on the pressure side of the wing E2 and tests were made at low and at medium wind speed. At speeds under approximately 2 ft./sec., the smoke remained laminar and helical streamline directions were seen round the main vortex cores. The secondary separation and other features of the flow discussed in Section 5.2 were also seen but no good photographs were obtained.

At a wind speed of 80 ft./sec., the smoke dispersed and found its way into the main vortex cores. This is shown in Fig. 23 for the wing E2 at 15-deg. incidence. The photograph was taken from the working section roof and the vortices are silhouetted downstream of the wing against a piece of black paper on the tunnel floor. The curvature of the vortex lines is consistent with the picture of Fig. 20.

Oil.

The surfaces of the wings E1, E2 were coated with emulsified (white) oil and patterns like that of Fig. 24 were obtained on the suction sides. Fig. 24 is a photograph of E2 at 15 deg. incidence taken some time after the airstream was started. The streamlines of the oil flow are clearly visible. A line of inflexions is seen to lie beneath the main vortex cores and an accumulation of oil is noticeable at the secondary separation lines. A narrow region just inboard of each leading edge was clear of oil. This is where it is thought that reattachment of the flow has taken place. When the wing was yawed through 10 deg. this band was wider at the attacking edge and careful inspection showed oil streamlines directed towards the leading edge thus lending support to the model of the flow described in Section 5.2.

The pictures taken with wings E1 and E2 were almost identical at moderate and large angles of incidence.

(iv) Paraffin and Chalk.

The model E2 was painted with a mixture of paraffin and chalk and tested at various angles of incidence and sideslip at a wind speed of 140 ft./sec. A typical photograph ($\alpha = 20$ deg.) is shown in Fig. 25. It was noted that the chalk pattern remained symmetrical about the root chord up to and including an angle of incidence of 50 deg. At 57 deg. incidence the pattern was quite irregular. It appears that, for a large range of incidence, the sharp leading edges of the wing enforce symmetry of flow which is absent for slender bodies of revolution at large angles of incidence.

7. Concluding Remarks.

Experiments have been made which have helped to form a consistent picture of the flow past slender delta wings at incidence. It would be useful to know more about the distribution of vorticity on the

suction side of such wings. The mechanism of what is described as secondary separation and reattachment of the cross-flow also needs further study. Without such knowledge it is impossible to decide how much these results are subject to Reynolds number effect. Theoretical models of the Legendre type are promising but the experiments have brought out the need for improvements which lead to more accurate prediction of the vortex position.

8. *Acknowledgments.*

D. I. Ainley and A. J. Taylor-Russell helped to make some of the measurements.

REFERENCES

<i>No.</i>	<i>Author(s)</i>	<i>Title, etc.</i>
1	R. Legendre	Flow in the neighbourhood of the apex of a highly swept wing at moderate incidences. (<i>La Recherche Aeronautique</i> No. 30, 1952, Nos. 31 and 35, 1953). Translated by Sylvia W. Skan. (May, 1954). A.R.C. 16,796.
2	R. H. Edwards	Leading-edge separation from delta wings. <i>J. Aeronaut. Sci.</i> , Vol. 21, 1954, pp. 134–135.
3	C. E. Brown and W. H. Michael, Jr.	Effect of leading-edge separation on the lift of a delta wing. <i>J. Aeronaut. Sci.</i> , Vol. 21, 1954, p. 690, 694 and 706.
4	T. Ornberg	A note on the flow around delta wings. K.T.H. Aero. Tech. Note 38, February, 1954.

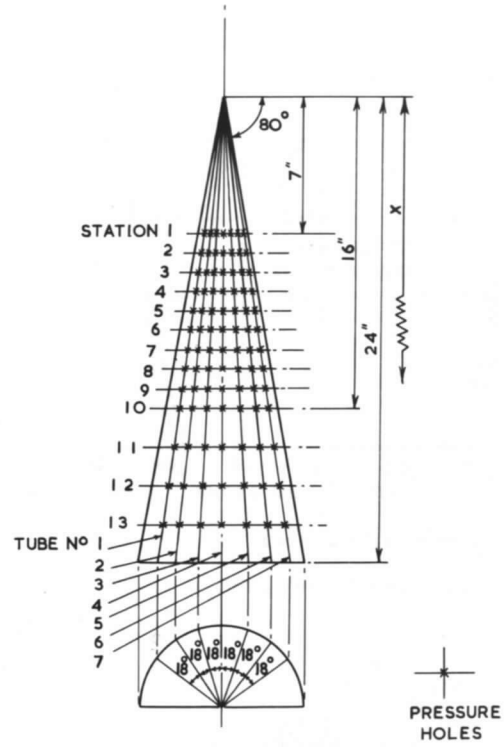


FIG. 1. Location of pressure holes in model E1.

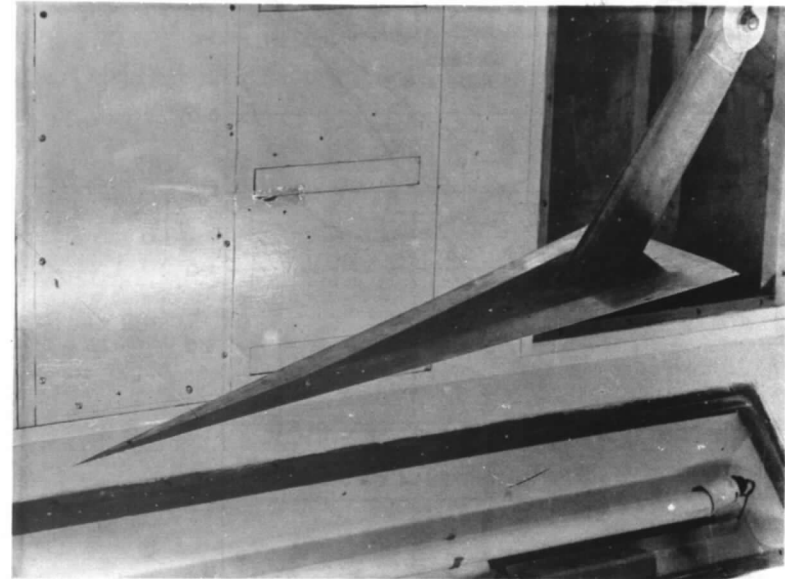
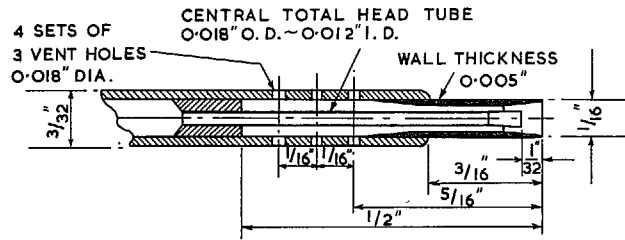


FIG. 2. Model E2 mounted.



VENT AREA \cong INLET AREA

KIEL TYPE TOTAL HEAD TUBE

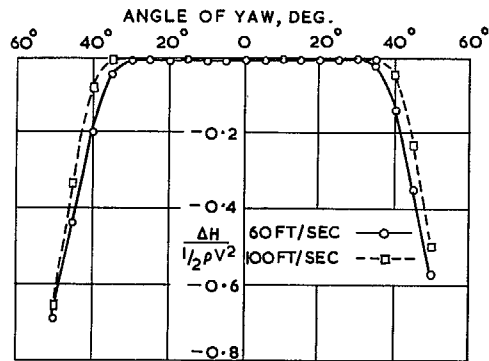


FIG. 3. Calibration curve for kiel tube.

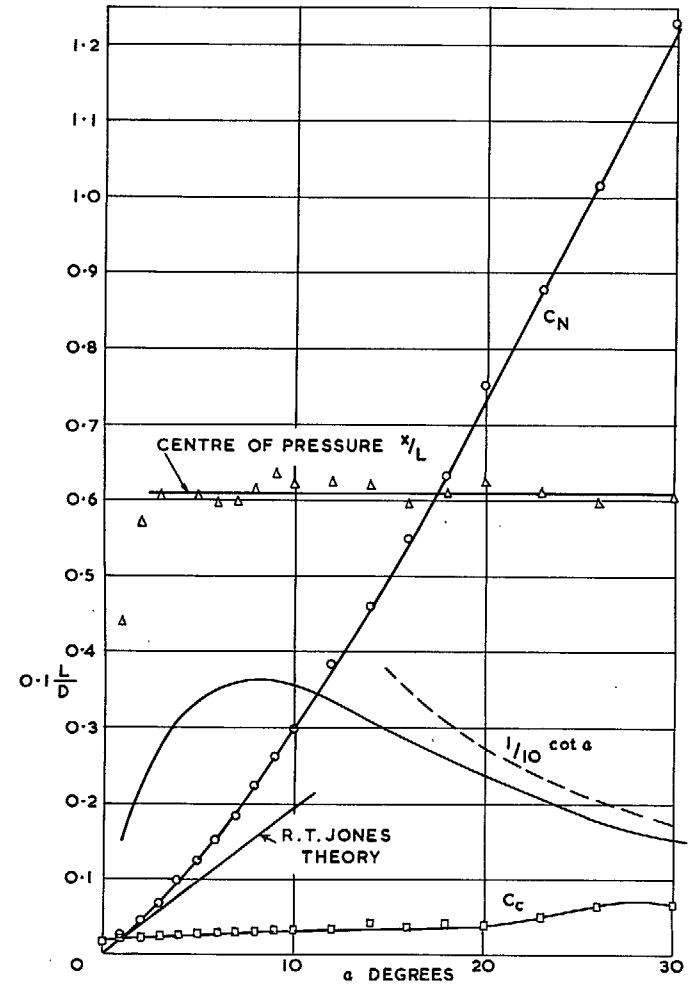


FIG. 4. Balance measurements. Model E1 speed 80 ft./sec.

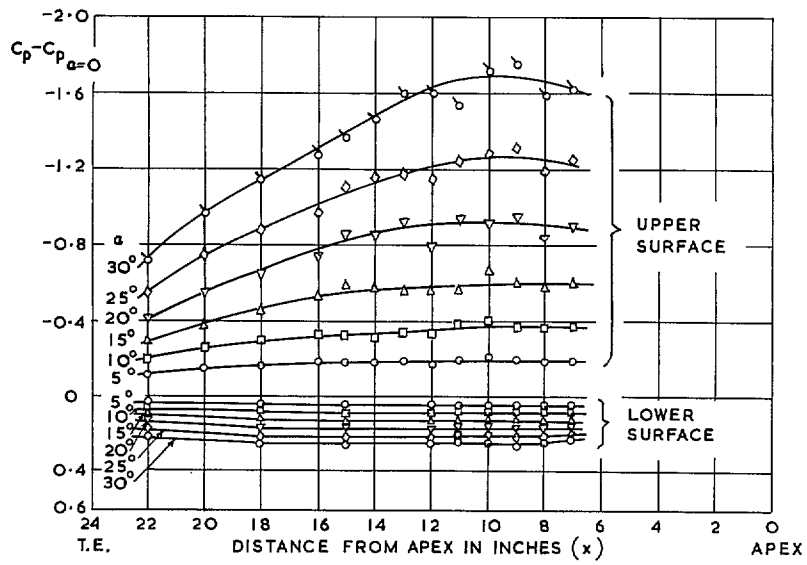


FIG. 5. Pressure distribution along generator No. 1, Model E1.

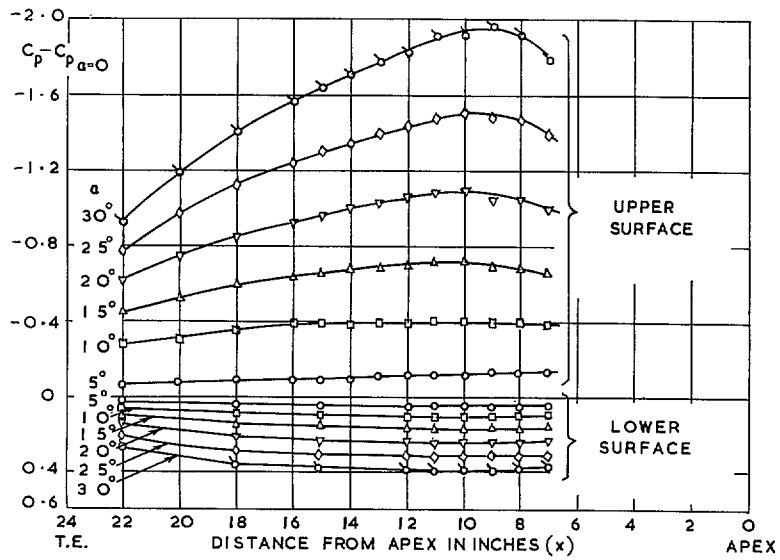


FIG. 6. Pressure distribution along generator No. 2, Model E1.

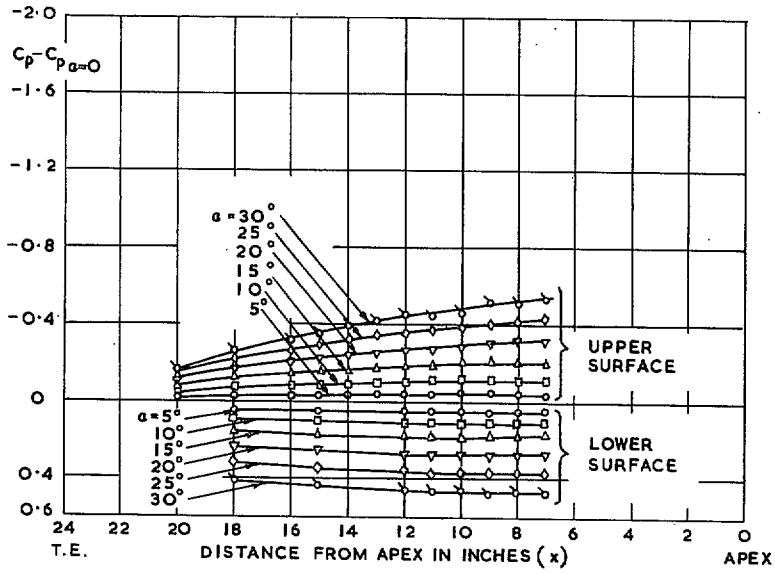


FIG. 7. Pressure distribution along generator No. 3. Model E1.

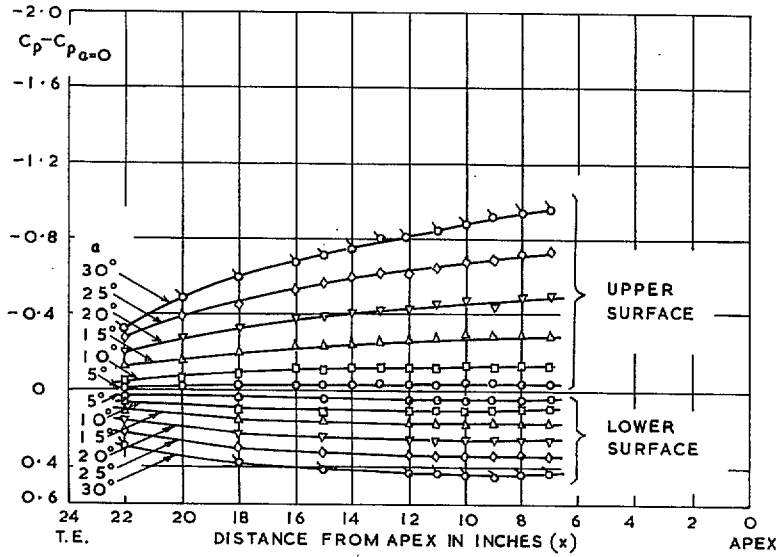


FIG. 8. Pressure distribution along generator No. 4. Model E1.

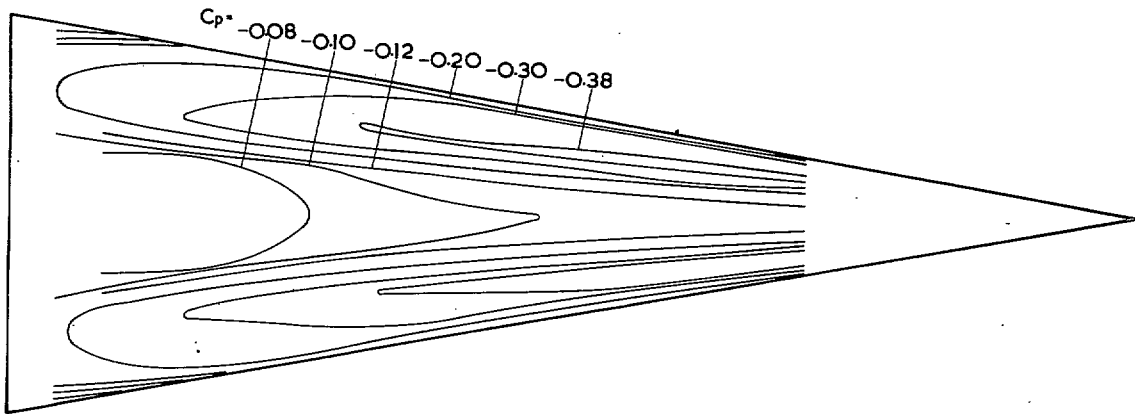


FIG. 8a. Wing E1: isobars on suction side at $\alpha = 10$ deg.

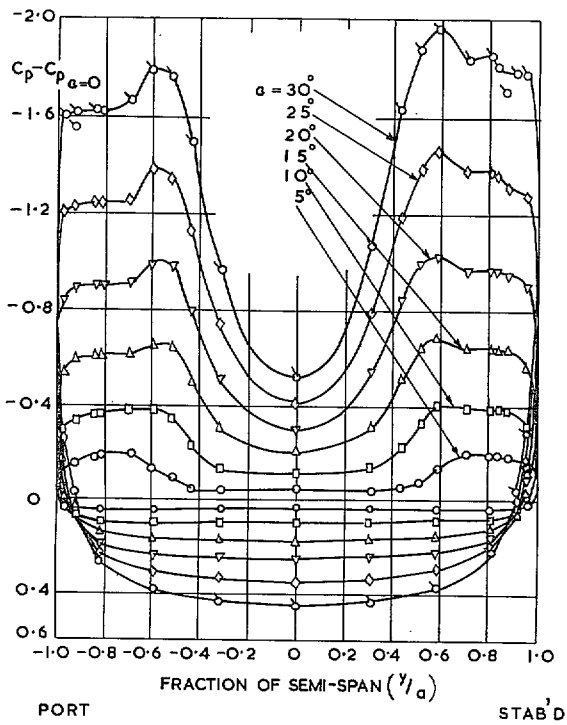


FIG. 9. Pressure distribution at Station 1. Model E1.

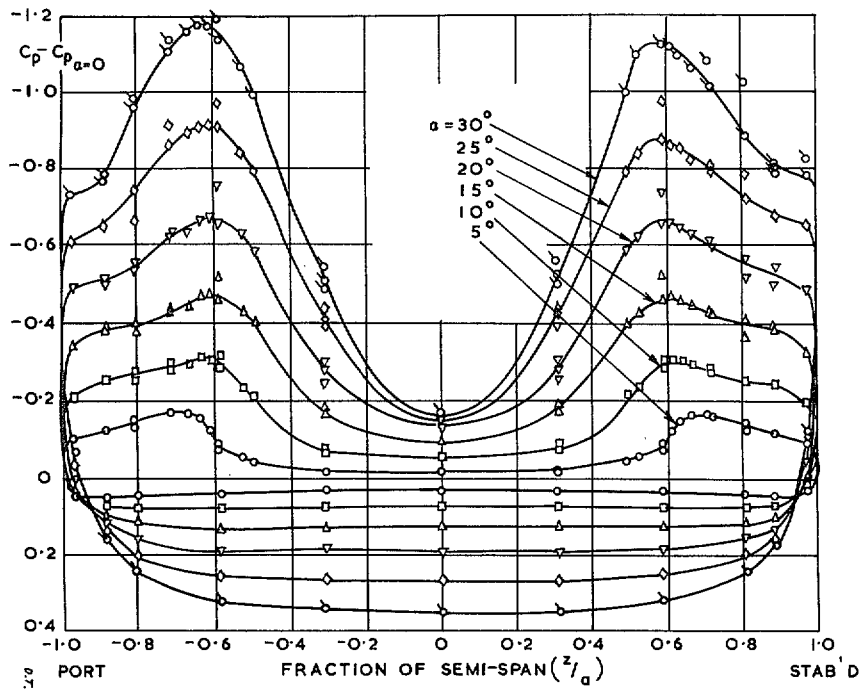


FIG. 10. Pressure distribution at Station 12, Model E1.

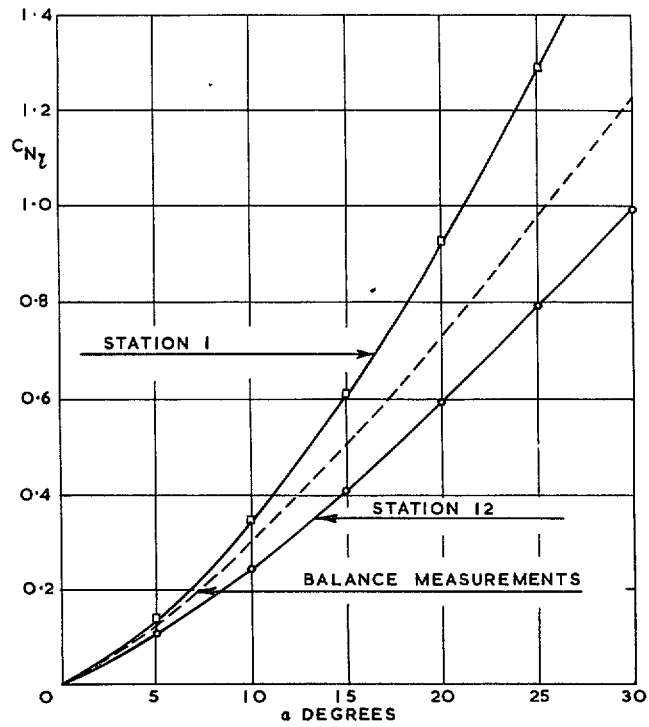


FIG. 11. Normal force coefficients at Stations 1 and 12, Model E1 speed 80 ft./sec.

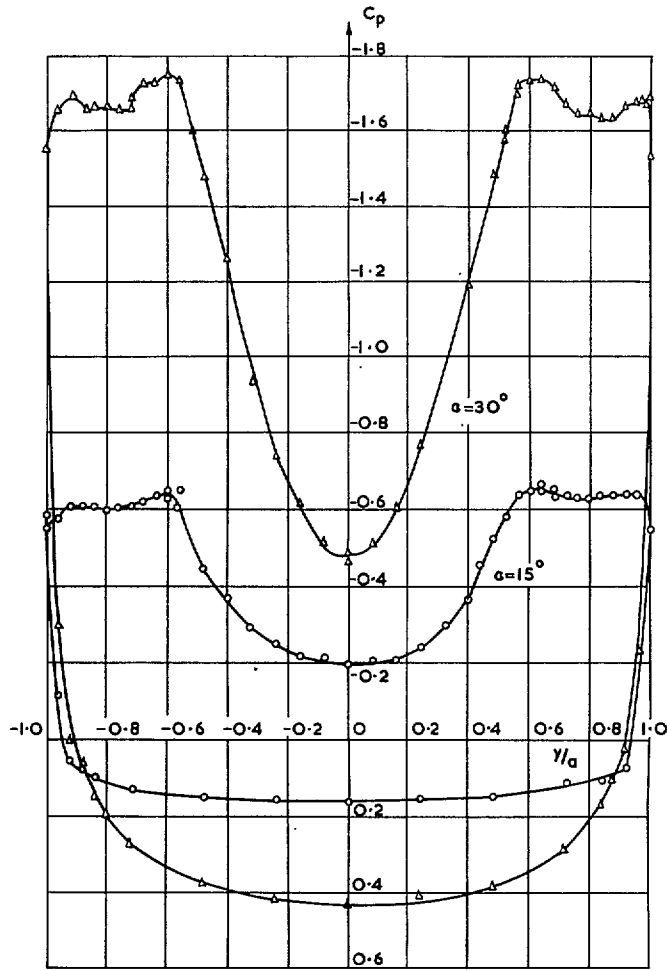


FIG. 12. Pressure distribution at Station 1. Wings E2.

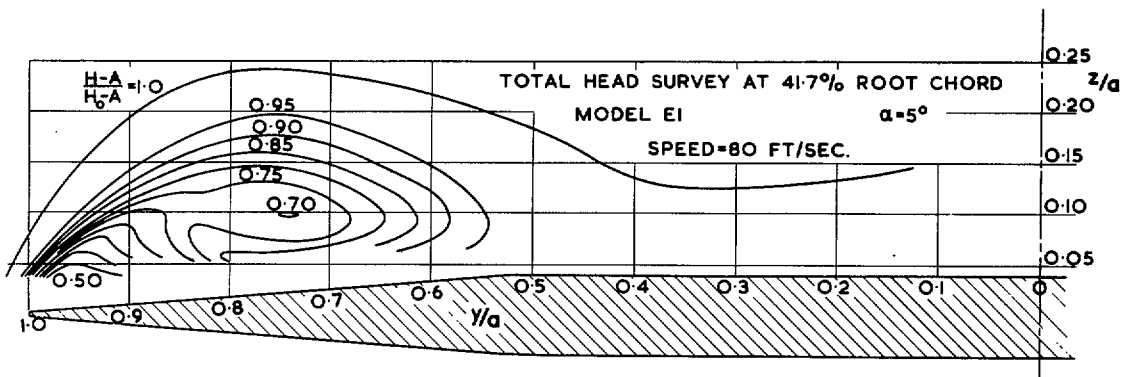


FIG. 13.

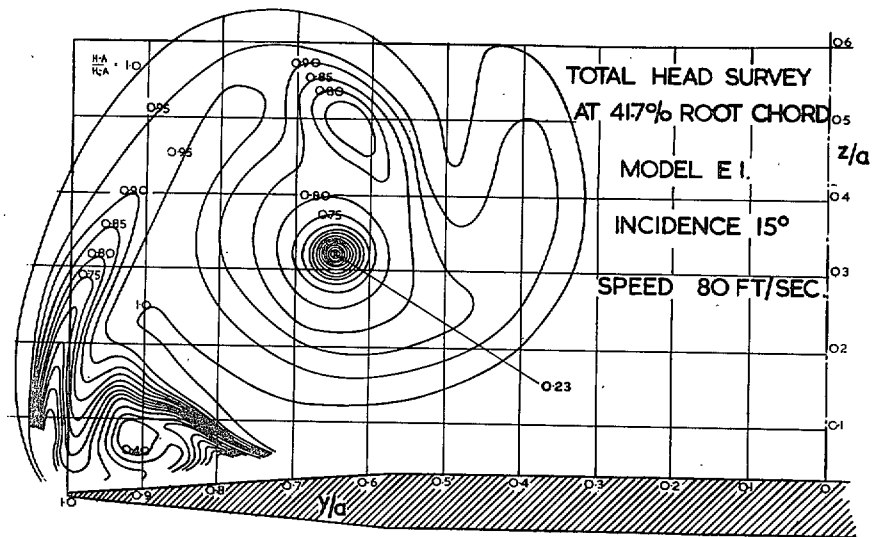


FIG. 14.

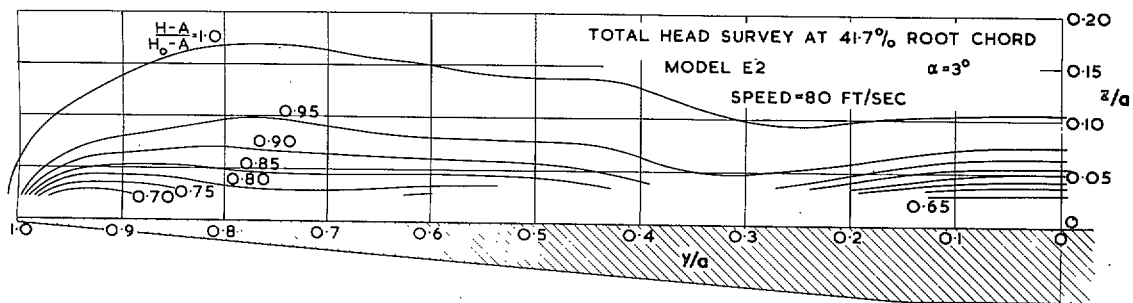


FIG. 15.

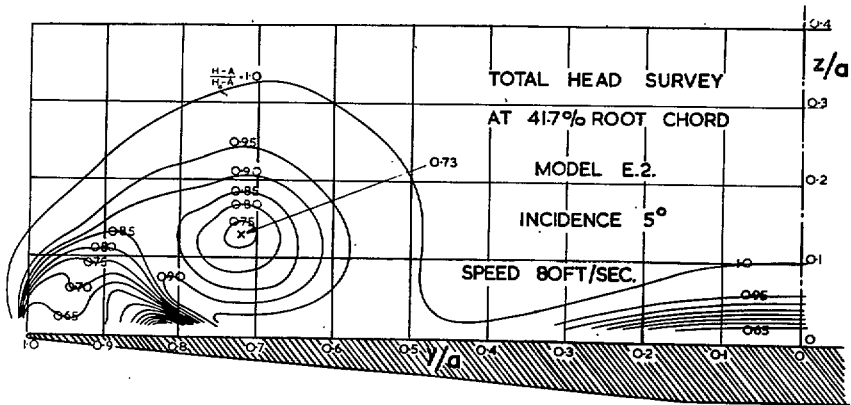


FIG. 16.

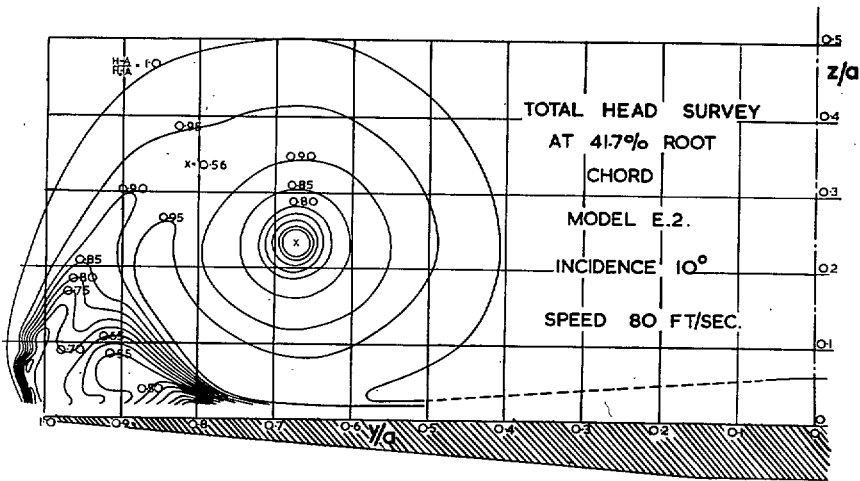


FIG. 17.

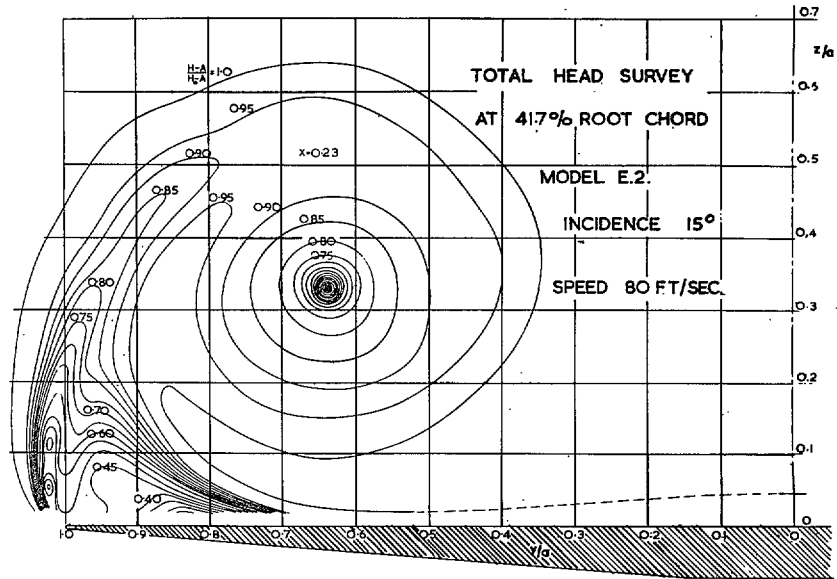


FIG. 18.

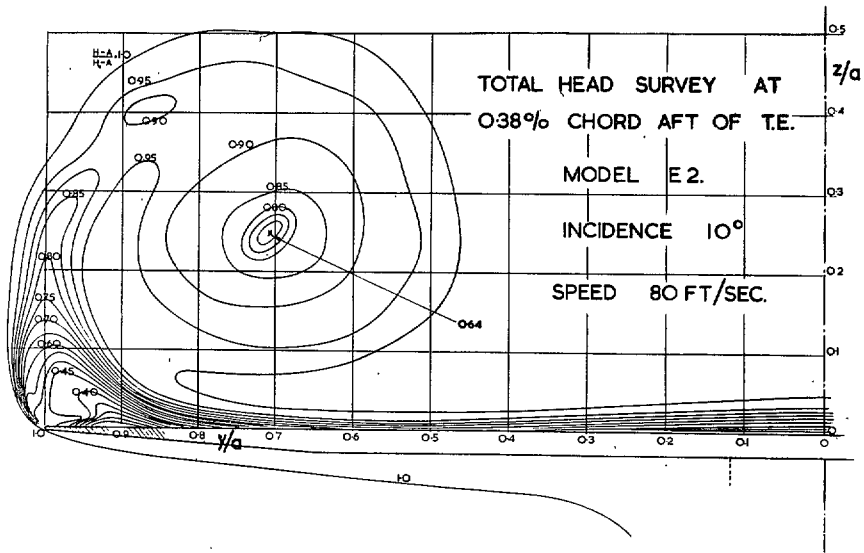


FIG. 19.

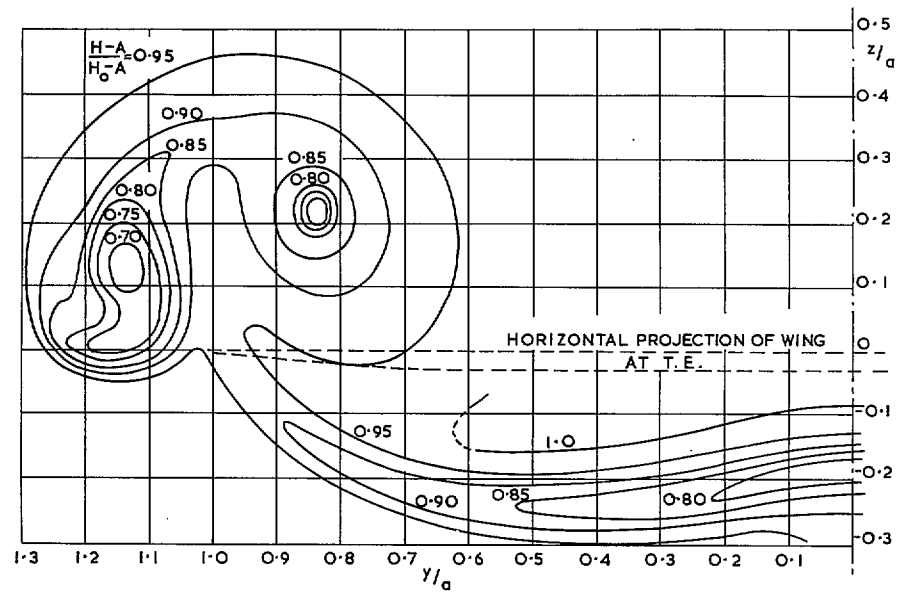


FIG. 20. Total head survey at 24 per cent chord aft of T.E. Model E2. Incidence 10° . Speed 80 ft./sec.

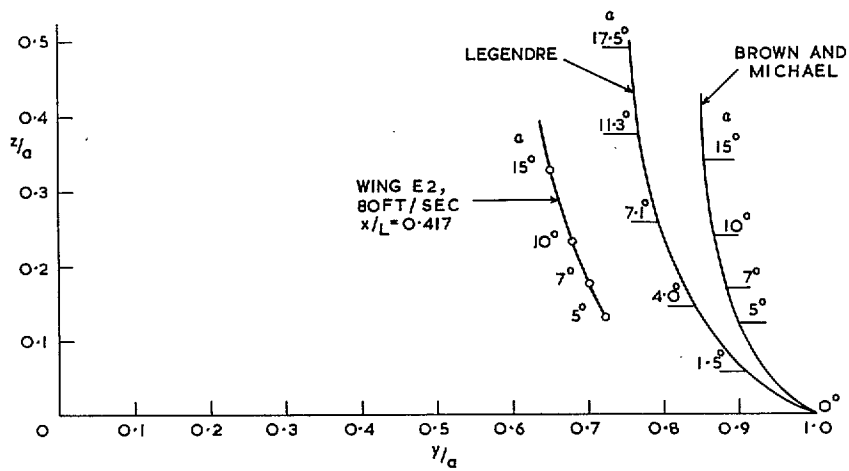


FIG. 21. Effect of incidence on vortex position.

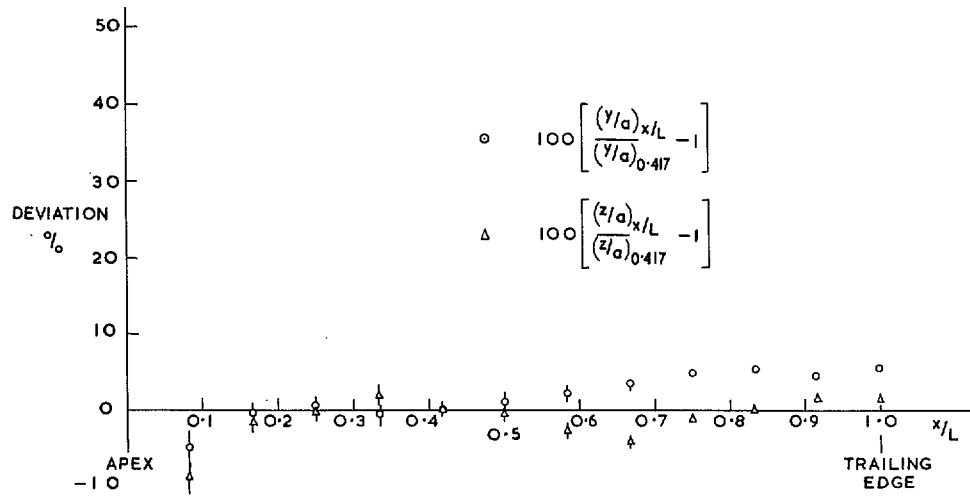


FIG. 21a. Wing E2: position of vortex cores for $\alpha = 10$ deg.

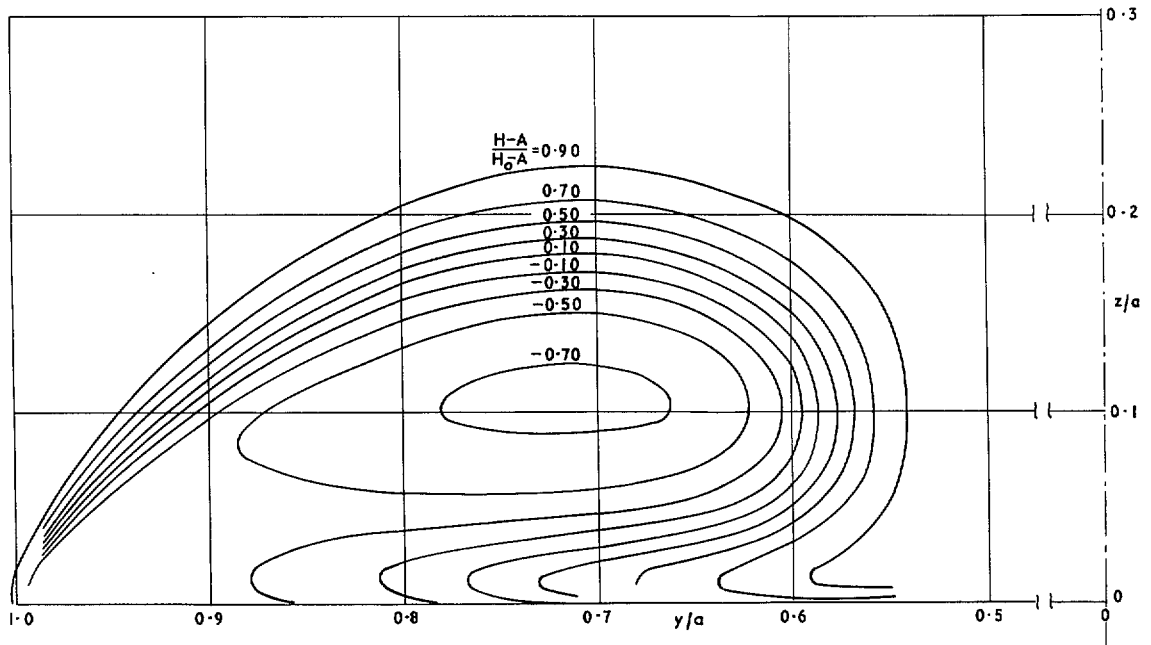


FIG. 21b. Total head survey at trailing edge. Model D. Incidence 15° . Speed 80 ft./sec.

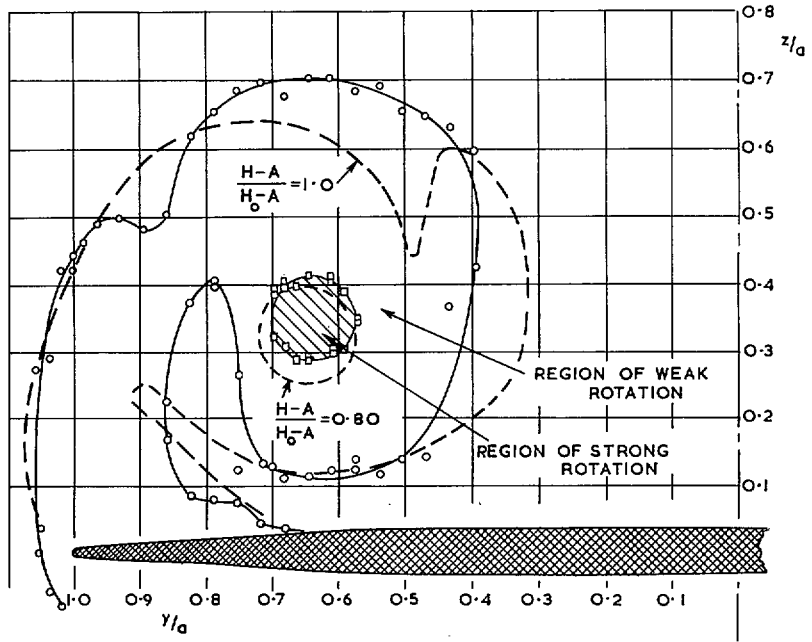


FIG. 22. Flow visualisation with tufts at 41.7 per cent root chord. Model E1, $\alpha = 15$ deg.
Speed = 80 ft./sec.

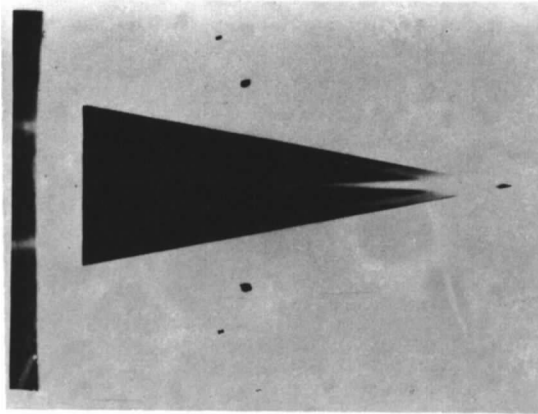


FIG. 23. Flow visualisation with smoke.

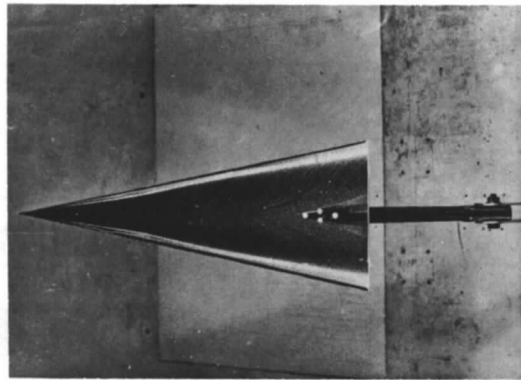


FIG. 24. Flow visualisation with oil.

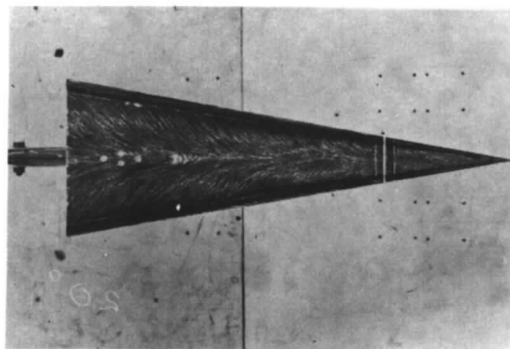


FIG. 25. Flow visualisation with paraffin-chalk mixture.

Part III.—Further Experiments with 20 deg. Delta Wings

By P. T. FINK

LIST OF CONTENTS

Section

1. Introduction
2. Spanwise Distribution of Chord Loading
3. Interpretation of Vortex Core Position
4. Measurements of Circulation in a Plane Downstream of the Wing
5. Experiments with Yawed Delta Wings

1. *Introduction.*

The recent appearance of Mangler and Smith's¹ theoretical analysis of the flow past slender delta wings with leading edge separation has encouraged the writer to note down the results of some experiments which are supplementary to those reported in Part II. The notation used here is that of Ref. 1. Some preliminary results of experiments with yawed delta wings are also presented.

2. *Spanwise Distribution of Chord Loading.*

Dr. Küchemann² has given an argument to show that a spanwise plot of the distribution of load ahead of a chord station has zero slope at the leading edges when these are lines of separation. Mangler and Smith have worked out examples of the load distribution for conical flow for various values of their incidence ratio α/K and a comparison with experiment has been obtained by assuming a conical pressure distribution corresponding to that which was observed at the forward Station 1 on the sharp-edged delta wing E1 (Ref. 2). The values are given in Table I and plotted in Fig. 1. The correspondence with the theoretical values is indifferent for $\alpha/K = 0.5$ and 1.0 but is remarkably close for $\alpha/K = 2.5$. The theoretical spanwise pressure distribution for the latter case is much less peaky than that which is predicted for smaller incidence (Fig. 7 of Ref. 1) and its form, if not the magnitude of its ordinates, corresponds to that which has been observed experimentally.

3. *Interpretation of Vortex Core Position.*

The total head surveys in planes perpendicular to the flow (see Part II) have minima at the cores of vortices. The spanwise position of these minima is compared with the positions of the 'core centres' of Mangler and Smith in Fig. 5 of their report¹ and the latter are found to be outboard of the experimental minima of total head by the following percentages of the semi-span:

α/K	0.4	0.8	1.2	1.6
%	16	12	10	8

The writer has used some unpublished work by D. A. Kirby to estimate the spanwise separation of

an experimental minimum of total head and of the corresponding centroid of vorticity found by taking first moments of area of suitably placed strips on an experimentally determined vorticity contour map. The centroid was found to be 8.5 per cent of semi-span outboard of the total head minimum at a chord station upstream of the trailing edge of a slender wing with slightly rounded leading edge at $\alpha/K = 2.8$.


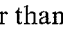
These contours of Kirby were also integrated to find the circulations round certain circuits for $\alpha/K = 2.8$. The vortex core was arbitrarily taken to be the region within the outermost nearly circular vorticity contour. (This agreed well with the outermost nearly circular total head contour.) The core so defined contained only 25 per cent of the net positive vorticity found at the chord station in question. The region of secondary separation contained -2.8 per cent of the above vorticity.

4. Measurements of Circulation in a Plane Downstream of the Wing.

The final statement of the previous section shows that the circulation associated with secondary separation is not likely to be appreciable for $\alpha/K = 1$ and this had been thought when interpreting the experimental results which were given in Part II. The Fig. 20 of that paper is a total head survey taken at one quarter chord downstream of the trailing edge. This traverse showed two regions of appreciably low total head per side and in view of the supposed weakness of the secondary separation vorticity, it was—erroneously—concluded that the rotation in both regions was in the same sense. Professor Collar questioned the validity of this and further measurements were made in March 1956 with the help of Mr. A. J. Taylor-Russell.

The wing E2 described in Part II had been lengthened and the root chord increased from 24 in. to 36 in. This was used at $\alpha = 9^\circ 54'$ ($\alpha/K = 1.0$) in the 5 ft. \times 4 ft. wind tunnel at 80 ft./sec. and is now referred to as wing E4.

The increased chord length made it necessary to repeat the total head survey in question and the results are given in Fig. 2. The survey is similar to that which was obtained behind the wing E2 (Fig. 20, Part II) but the secondary total head minimum of the latter test was now replaced by a pair of minima outboard of the leading edge vortex. Further traverses were then made with a 5-hole probe and with a static pressure tube in order to make it possible to evaluate the circulation round the circuits which are marked by the heavy lines of Fig. 2. The values of the circulation are also given there, expressed as fractions of the net circulation round a circuit which encloses all the other circuits shown.

It was evident that there was substantial rotation in a sense opposite to that of the leading-edge vortex. In fact for every three units of positive vorticity, there was about one unit of negative vorticity and it was then realised that the vorticity shed at the trailing edge may have been of unconventional sign. The late Professor H. B. Squire suggested a bound vortex pattern* which agreed qualitatively with that which was later worked out by Mangler and Smith and given in Fig. 12 of their report¹. It was argued from this that when the vortex sheet shed at the trailing edge is of opposite sign to that usually found, the sheet rolls up like (i)  rather than like (ii) . The configuration (i) is strongly influenced by the leading-edge vortices whose effect is to sweep the trailing-edge cores out and up. Maltby's experiments with smoke seem to bear this argument out. Mr. Maltby kindly supplied the photograph shown in Fig. 3a. This was taken in a plane normal to the stream at 30 per cent of root chord downstream of the trailing edge of a slender delta wing operating at an incidence ratio $\alpha/K = 1.4$.

Mangler and Smith have tabulated the proportions of trailing vorticity originating in various ways according to their theory (see Table II of Ref. 1) and the above measurements may be used for a comparison. They predict that at $\alpha/K = 1.0$, the proportion of vorticity leaving the wing in the usual sense is 77 per cent. The present experiment—made at 80 ft./sec. (non-conical flow) gave 69 per cent. This is considered to be a close agreement.

*As shown in Fig. 3b this pattern of bound vortex lines evolved in a discussion of possible shapes which would correspond to a high loading under the vortices and a lower loading elsewhere on the wing.

5. Experiments with Yawed Delta Wings.

Some preliminary work with yawed delta wings was completed early in 1956 and will be outlined here. A more complete study was later undertaken at Imperial College by J. K. Harvey.³

Surface flow patterns indicated the expected result that the effect of yaw was to produce asymmetry in the position of the leading-edge vortices and in the associated flow. The region of secondary separation near the attacking edge is wider than in the unyawed case. Thus there is better promise of successful experimental investigation in this region. The Fig. 4 shows total head contours near the attacking edge at an angle of sideslip (β) of 10 deg. ($\beta/K = 1.0$) and at $\alpha = 10$ deg. ($\alpha/K = 1.0$).

The shape of the contours may be compared with those of Fig. 17 of Part II which relates to the corresponding unyawed case. The main vortex core is seen to have moved down towards the wing and inboard ($y/a = 0.52$, $z/a = 0.2$ compared with $y/a = 0.68$, $z/a = 0.24$ for the unyawed wing). The corresponding core on the leeward side—not shown in the figure—is at $y/a = -0.9$, $z/a = 0.4$; i.e. this is a weak vortex which is nearly 'blown off' the leeward leading edge. The secondary separation line in Fig. 4 is approximately 0.08 of a semispan outboard of the primary core. This is similar to the result for the unyawed wing.

Some spanwise measurements of surface static pressure were made with the lengthened wing E4 at a station $x/c = 0.4$. The results are plotted in Figs. 5 and 6. The effect of the yaw in changing the position of the vortices is clearly seen in the distributions. The distribution of pressure on the pressure side of the wing is characterised by a peak near the attacking edge. This is at an attachment line which is analogous to the front stagnation point in the corresponding two-dimensional flow.

It was found that the local lift coefficients obtained by integration of the curves were independent of sideslip for $\alpha = 10$ deg., but decreased somewhat with β at $\alpha = 5$ deg. The range tested $\beta/K = 1.0$.

The following values for the local rolling moment coefficient were obtained by integration.

	$\beta = 0$ deg.	$2\frac{1}{2}$ deg.	5 deg.	10 deg.
$\alpha = 5$ deg.	0.0014	0.0099	0.018	0.029
$\alpha = 10$ deg.	0.0013	—	0.0275	0.0545

The experimental values of $1/\alpha [C_l - C_{l\beta=0}]$ are plotted against $v \cdot \beta$ in Fig. 7.

A theoretical relation is also shown. However, this is derived from Ribner's slender wing evaluation for attached flow. Ribner's value $C_l = -\pi\alpha\beta/3$ is shown multiplied by 3/2 in order to make it possible to compare his total wing estimate with the present local coefficients. The discrepancy is surprisingly small and would be expected to be still less in a comparison with low speed balance measurements.

REFERENCES

- | <i>No.</i> | <i>Author(s)</i> | <i>Title, etc.</i> |
|------------|-------------------------------------|---|
| 1 | K. W. Mangler and
J. H. B. Smith | Calculation of the flow past slender delta wings with leading-edge separation.
A.R.C. 19,634, May, 1957. |
| 2 | D. Küchemann | A non-linear lifting-surface theory for wings of small aspect ratio with edge separations.
A.R.C. 17,769, April, 1955. |
| 3 | J. K. Harvey | Some measurements on a yawed slender delta wing with leading edge separation.
A.R.C. R. & M. 3160, October, 1958. |

TABLE I

Spanwise Distribution of Chord Loading

—
Values of $\frac{KL(y)}{sC_N}$, $K = \tan^{-1} 10^\circ$

<i>y/s</i>	0.05	0.15	0.25	0.35	0.45	0.55	0.65	0.75	0.85	0.95	1.00
$\alpha = 5^\circ$	0.695	0.671	0.640	0.622	0.604	0.592	0.537	0.506	0.220	0.037	0
$\alpha = 10^\circ$	0.679	0.679	0.702	0.717	0.685	0.584	0.445	0.298	0.159	0.026	0
$\alpha = 25^\circ$	0.698	0.743	0.773	0.756	0.662	0.535	0.407	0.260	0.141	0.022	0

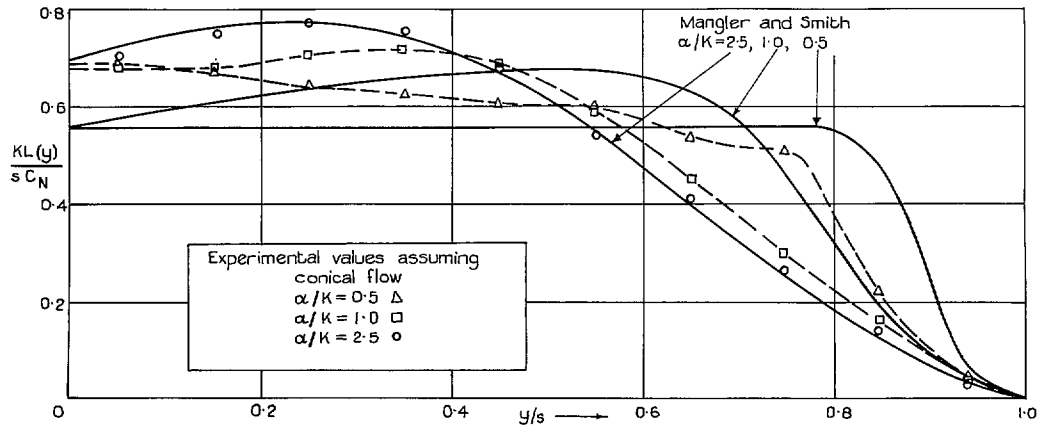


FIG. 1. Spanwise distribution of chord loading.

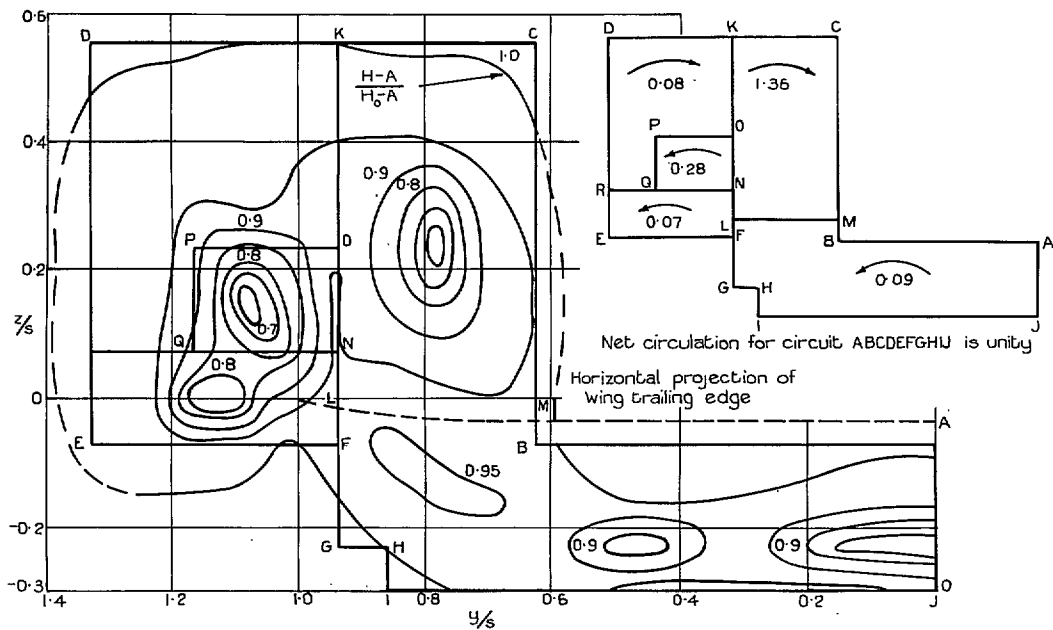


FIG. 2. Total head survey and circuits for measurements of circulation at 25 per cent aft of T.E. Model E4. incidence 10° ($\alpha/K = 1.0$) speed 80 ft./sec.



FIG. 3. Smoke visualization of flow behind slender delta wing (Maltby) $\alpha/K = 1.4$, $x/c = 1.3$

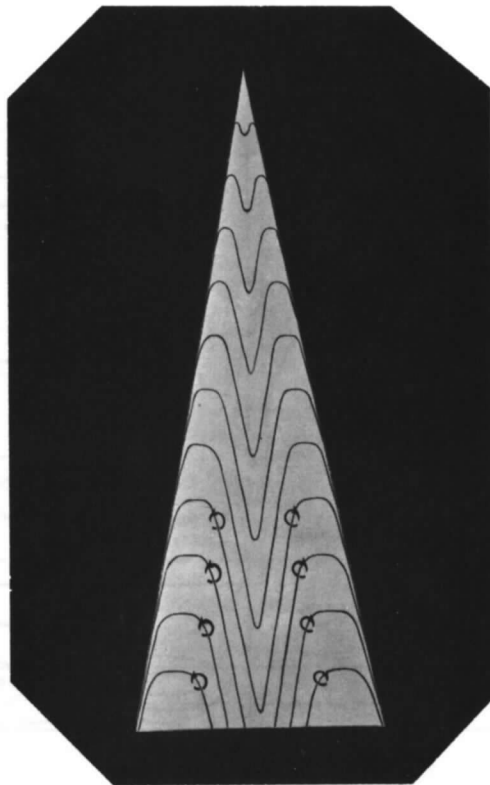
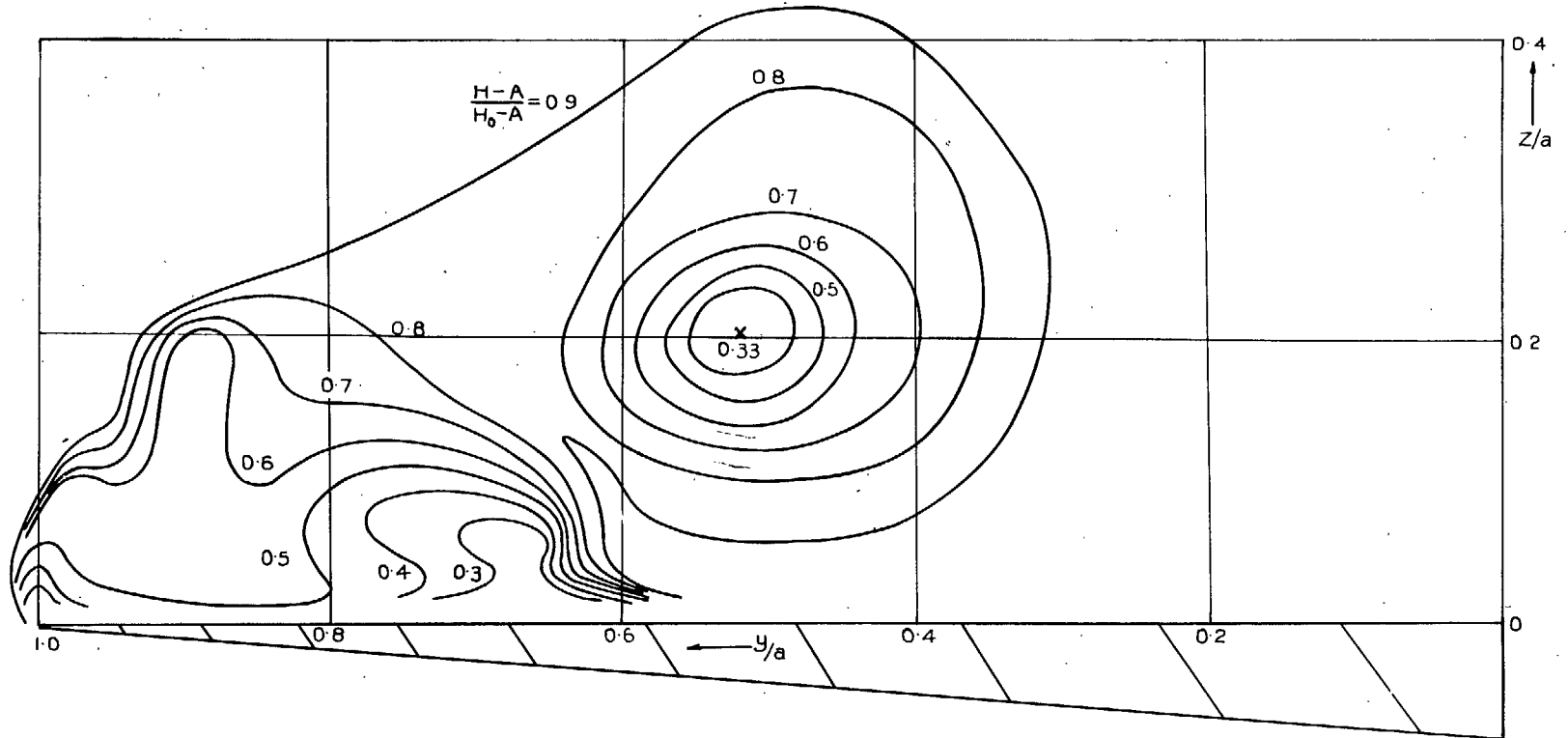
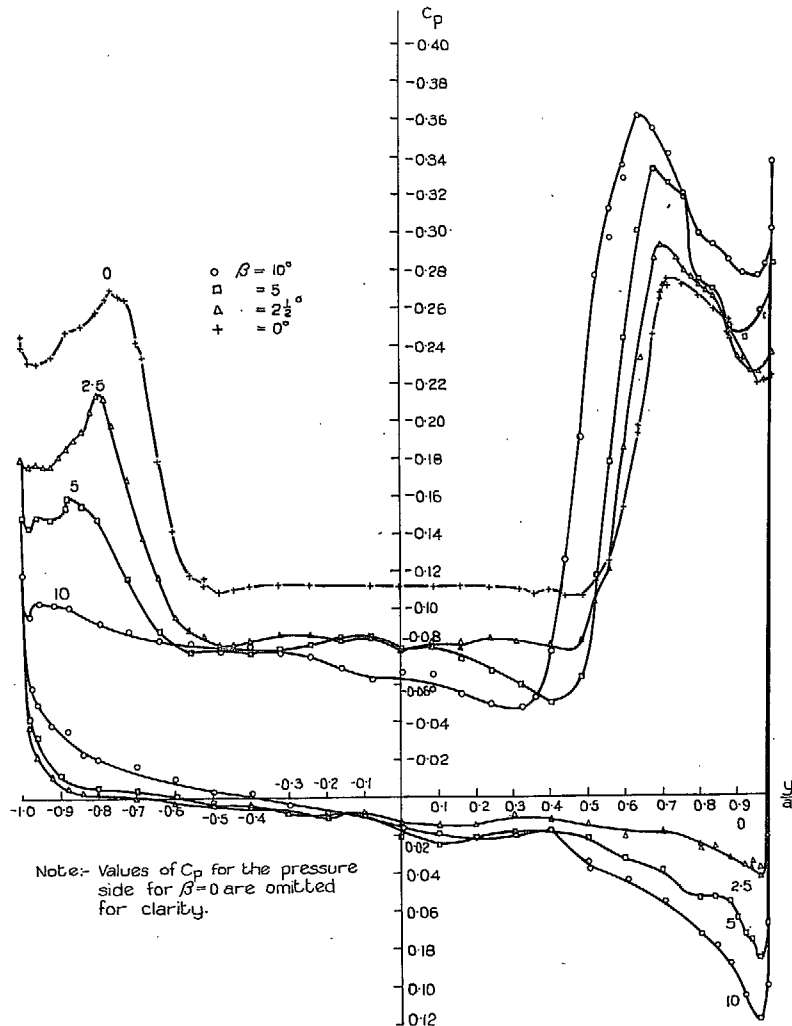


FIG. 3b. Schematic of Bound Vortex Pattern for Consistency with Loading.



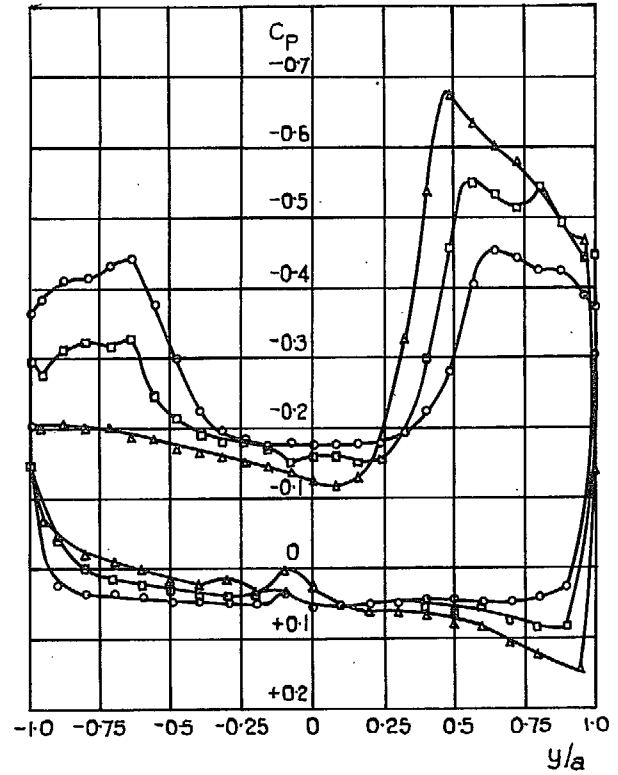
Model E2, incidence 10° ($\frac{\alpha}{K} = 1.0$), yaw 10° ($\frac{\beta}{K} = 1.0$), station 7.1 in. ($\frac{x}{C} = 0.295$), speed 80 ft./sec.

FIG. 4. Total head survey near attacking edge of yawed slender delta.



Pressure distribution at $\frac{x}{C} = 0.4$. Wing E4, incidence 5° ($\alpha/K = 0.5$) speed 80 ft./sec.

FIG. 5. Yawed slender delta.



Leading edge sweep = 80°

$\alpha = 10^\circ$ $\beta = 0^\circ$ \circ
 $\alpha/K = 1.0$ $\beta = 5^\circ$ \square
 $\beta = 10^\circ$ \triangle

FIG. 6. Spanwise pressure distribution on yawed Delta wing.

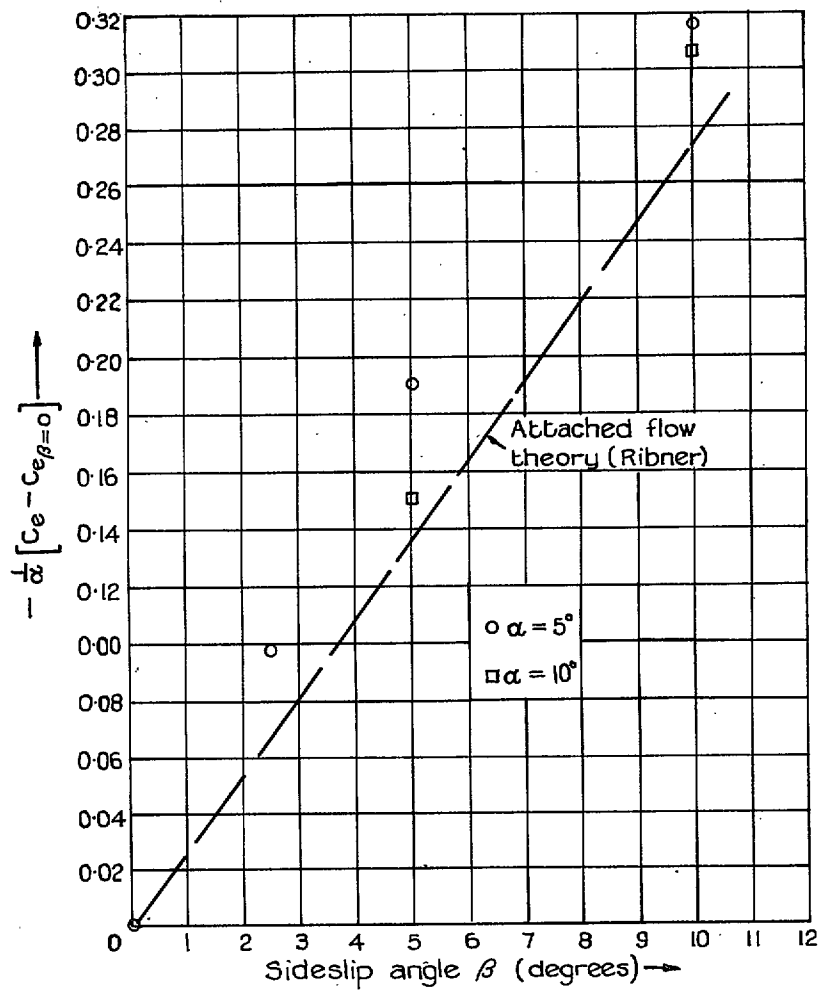


FIG. 7. (Local) rolling moment due to sideslip.

© *Crown copyright* 1967

Published by
HER MAJESTY'S STATIONERY OFFICE

To be purchased from
49 High Holborn, London w.c.1
423 Oxford Street, London w.1
13A Castle Street, Edinburgh 2
109 St. Mary Street, Cardiff
Brazennose Street, Manchester 2
50 Fairfax Street, Bristol 1
35 Smallbrook, Ringway, Birmingham 5
80 Chichester Street, Belfast 1
or through any bookseller